



Technology Milestone Whitepaper

EXCEDE Technology Milestone #2: Broadband Contrast Demonstration Final Report

Glenn Schneider¹ (PI), Julien Lozi², Olivier Guyon, Kevin Newman
(The University of Arizona)

Ruslan Belikov, Dan Sirbu, Dana Lynch, Peter Zell
(NASA/Ames Research Center)

Sandrine Thomas³, Eugene Pluzhnik, Fred Witteborn
(NASA/Ames Research Center [UARC])

Eduardo Bendek
(NASA/Ames Research Center [BAER])

Troy Hix, Alison Nordt
(Lockheed-Martin Advanced Technology Center)

September 22, 2015

JPL Document D-95432

National Aeronautics and Space Administration
Jet Propulsion Laboratory
California Institute of Technology
Pasadena, California

© 2015 copyright. All rights reserved.

¹ contact: gschneider@as.arizona.edu, Steward Observatory, 933 N. Cherry Ave. Tucson, AZ 85721 USA

² current affiliation: Subaru Telescope

³ current affiliation: Large Synoptic Survey Telescope

Approvals:

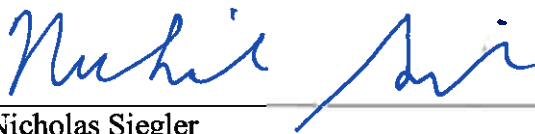
Released by



22 September 2015

Glenn Schneider
Principal Investigator

Date



10/2/15

Nicholas Siegler
Exoplanet Exploration Program Technology Manager

Date

Douglas Hudgins
Exoplanet Exploration Program Scientist, NASA HQ

Date

PLACEHOLDER FOR EXEP SIGNATURES

TABLE OF CONTENTS

Cover Page	1
Signature/Approvals Page	2
Table of Contents.....	3
1. Introduction to the EXCEDE Technology Maturation & Demonstration Investigation	4
1.1 Prior Key Documents	4
1.2 From Air to Vacuum, and From Monochromatic to Broadband Light.....	5
1.3 Modeling and Interpretation of Milestone #2 Test Results	6
2. Description of Milestone #2	7
3. Laboratory Configuration.....	8
3.1. Overview.....	8
3.2. Vacuum Chamber and Test Bed Facility.....	8
3.3. Optical Configuration	10
4. EXCEDE Vacuum Chamber Tests: Schedule and Goals.....	13
5. EXCEDE MS #2 Vacuum Test Bed System Calibration.....	14
5.1. Deformable Mirror Calibration.....	14
5.2. Input Fiber Alignment.....	16
5.3. Inverse PIAA Alignment and Image Scale	17
5.4. Contrast Calibration	18
5.5. Focal Plane Mask Alignment and Inner Working Angle Verification	19
5.6. Low Order Wavefront Sensor (LOWFS) Calibration	20
6. Milestone #2 Demonstration	22
6.1. Milestone Procedure	22
6.2. Milestone #2 Data Collection	23
7. Milestone #2 Results	24
8. Model Comparison	26
8.1. Model Description	26
8.2. Ideal Performance.....	27
8.3. Low Oder Aberrations	28
8.4. Simulation Results.....	29
8.4.1. Sensitivity to Tip/Tilt.....	30
8.4.2. Contrast Degradation with Increasing Bandwidth.....	31
8.4.3. Simulation Comparison of WF Control Algorithms.....	32
9. What Next? – Meeting the Milestone.....	33
10. Summary and Conclusion	35
11. References	36
Appendix A – EXCEDE Flight Proposal Science Traceability Matrix	38
Appendix B – Source Calibration Using the LOWFS	39
Appendix C – Certification Data Package	41
Appendix D – Comments on the Coronagraph Optical Model	44
Appendix E – Acronym List.....	45

1. Introduction to the EXCEDE Technology Maturation & Demonstration Investigation

The EXoplanetary Circumstellar Environments and Disk Explorer (EXCEDE; [Guy12]) is an Explorer program flight-mission concept designed to study the formation, evolution, and architectures of exoplanetary systems through direct imaging of starlight-scattering materials in circumstellar environments into stellar habitable zones; see § 1.2 of [Sch12]. The EXCEDE flight instrument is conceived as a two-band optical imaging polarimeter integrated with a high-performance stellar coronagraph and off-axis (unobscured pupil) 0.7 m diameter TMA telescope [Sch12a]. EXCEDE was selected as an Explorer program “Category 3” laboratory investigation to advance the maturity of key elements of its proposed starlight suppression system (SSS; see § 2.2 of [Sch15]). The charge to the EXCEDE project by NASA HQ was to “further mature appropriate elements of the EXCEDE technologies as outlined in Table F-5” [of the EXCEDE proposal]. Those elements being (simultaneously) use of: (1) PIAA optics for high contrast coronagraphy, (2) Deformable Mirror for mid-spatial frequency wavefront control, (3) Low-order wavefront sensing, (4) Wavefront control algorithms, (5) Complete integration of the SSS.

This EXCEDE technology maturation and demonstration (TM&D) program (both phases defined by technology milestones 1 & 2; see § 1.1) was carried out under the programmatic direction of Glenn Schneider (PI, UofA) and technical leadership of Ruslan Belikov (NASA/ARC).

1.1 *Prior Key Documents*

The first phase of our laboratory investigation addressed the integrated maturation of the above SSS elements used with monochromatic light, in a stabilized air environment, as documented in prior deliverable milestone (MS) reports to the NASA EXEP Office:

- (1) - “EXCEDE Technology Milestone #1: Monochromatic Contrast Demonstration” (JPL Document D-75789) [Sch12] and,
- (2) - “EXCEDE Technology Milestone #1: Monochromatic Contrast Demonstration Closure Report” (JPL Document D-81732) [Sch13].

This final report documents the conduction of, and results from, the second phase of our TM&D investigation, carried out in a vacuum environment, and with broadband light, as described in its predecessor document:

- (3) - “EXCEDE Technology Milestone #2: Broadband Contrast Demonstration” (JPL Document D-94365) [Sch15].

For brevity, and obviation of redundancy in this report, these prior documents (1) – (3) should be consulted as primary references to gain a detailed understanding of:

- (a) the overall objectives of the EXCEDE TM&D program including traceability to science requirements and mission goals,
- (b) an introduction to Phase Induced Amplitude Apodization (PIAA) coronagraphy and its applicability with wavefront error (WFE) sensing and control to the EXCEDE measurement and instrument requirements,

- (c) a description of the overall TM&D plan,
- (d) further rationale, definitions, and computations for ascertaining performance metrics,
- (e) S/W tools and processes developed for MS #1 and MS #2 testing,
- (f) criteria for evaluating, and procedures for documenting, performance,
- (g) other background and precursor information discussed therein.

1.2. From Air to Vacuum, and from Monochromatic to Broadband Light

Following the completion of MS#1 (in-air, monochromatic testing at the NASA/Ames Coronagraph Experiments (ACE) Laboratory [Bel12a, Bel12b]; see JPL Document D-81732), the TM&D program for EXCEDE MS #2 (vacuum environment, broadband testing) was conducted at the Lockheed-Martin (LM) Advanced Technology Center (ATC; Palo Alto, CA) using a vacuum Metrology Environment Test (“MET”) chamber facility in which the EXCEDE test bench was embedded and operated. The laboratory TM&D program for MS #2 was carried out from December 2013 – March 2015 in a vacuum environment germane to an EXCEDE low-earth-orbit flight mission. Modeling and analysis of test results continued through September, 2015.

In advancing from our MS #1 to MS #2 experimentation, per our TM&D plan, the EXCEDE SSS test bench was prepared/upgraded for vacuum environment operation [Ben14] and testing [Bel13a]. The system was also reconfigured for exploring broadband (up to $\Delta\lambda/\lambda = 10\%$) rather than monochromatic, contrast/working angle performance, in an optically more flight-like configuration [Bel13b]. In this phase, the EXCEDE instrument concept maturation benefited greatly from: (a) testing and verifying SSS operability and performance in a space-like vacuum environment and, (b) moving to a more flight-like optical configuration importantly including: (1) the placement of the deformable mirror (DM) at the front-end of the optical path and, (2) the incorporation of inverse PIAA optics – both conforming to the EXCEDE concept SSS/coronagraph flight configuration. See [Sch15] § 3.2 for a description of the LM PIAA vacuum laboratory (MS #2) configuration of the EXCEDE test bench, and [Sch15] § 3.3 for primary differences from MS #1 and flight configurations.

Our build-up and testing of the modified EXCEDE test bench for broad-band exploration in a vacuum environment was carried out, incrementally, in five runs in the LM MET vacuum environment test chamber; see Table 1. The latter two runs (following test bed build up with vacuum operability, functionality, and system calibration testing) provided: (in Vacuum Chamber Test; hereafter VCT, #4) initial insights in improving image contrast moving from monochromatic to broadband operation, and (in VCT #5) more narrowly designed for parametric exploration in system configuration and WFE control but conceived with rigor for establishing and demonstrating performance, repeatability, and systemic limitations.

Monochromatic performance that was earlier rigorously demonstrated for MS #1 in thermally stabilized air (see [Sch13]) was very closely replicated with the vacuum test bed reconfigured with the DM upstream of the PIAA optics, and the inclusion of the inverse PIAA system as tested in VCT #4 (see [Sch15] § 2.3). However, the system fell short of the MS#2 IWZ contrast goal in rigorous testing during the final vacuum demonstration test, VCT #5 (see § 7 of this report), although we believe we understand the reasons and are reasonably confident that only one more vacuum test would be required to achieve MS#2.

1.3. Modeling and Interpretation of Milestone #2 Test Results

For cost containment but with demonstration sufficiency, per our test plan, we re-used several key optical components available to the investigation. This included (importantly) PIAA optics, that were not optimized for broadband operation, but whose polychromatic and other effects could be analytically interpreted through modeling informed by experimentation, and with a post-facto understanding of the as-configured test-bed as operated; see § 8 & § 9.

We therefore importantly adopted an analytic approach, through modeling of the system, to reproduce and understand the experimental results obtained in VCT #5 – specifically, to determine the (still) limiting factor(s) in order to bring the system into MS #2 performance compliance with future revisions/augmentations to the end-to-end system. We discuss this modeling effort, and its results, in light of the test data, in detail in § 8 of this report.

2. Description of Milestone #2

This report documents the vacuum laboratory investigation toward the attainment of EXCEDE TM&D milestone #2, defined in JPL Document D-94365 to:

“Demonstrate, using a PIAA coronagraph with an inner working angle of $1.2 \lambda/D$, a raw contrast median level of 10^{-6} between 1.2 and $2 \lambda/D$, simultaneously with a median level of $\leq 3 \times 10^{-7}$ between 2 and $\geq 4 \lambda/D$, in broadband light at a central wavelength in the range $400 - 900$ nm and a spectral bandwidth $\Delta\lambda / \lambda$ of 10% over a single-sided dark zone⁴.”

In particular, for our test and demonstration specifically germane to the EXCEDE flight-mission concept, the test bench was configured and operated to provide a wavefront corrected outer working angle of $11 \lambda/D$ ⁵.

Thus, the two simultaneously controlled stellocentric nearly semi-annular zones were configured as:

IWZ (inner working zone): $1.2 - 2.0 \lambda/D$ (PIAA throughput increasing from 50% at $1.2 \lambda/D$)

OWZ (outer working zone): $2.0 - 11 \lambda/D$

For a central wavelength we adopted 650 nm, mid-way between the EXCEDE flight instrument concept's two (red and blue) spectral bands, and mid-range w.r.t. MS #2. For spectral bandwidth we explored the full range from monochromatic to the MS #2 goal of 10%.

The MS #2 raw median contrast level of $\leq 3 \times 10^{-7}$ (3x more demanding than the instrument functional requirement per the EXPLORER11 flight proposal; see science traceability matrix instrument functional requirements in Appendix A) in the OWZ (97.9% of the wavefront controlled area) at a 10% spectral bandwidth was attained (see § 7; Figure 11). However, the simultaneously controlled 10% bandwidth raw median contrast in the IWZ (the first 0.8 resolution elements, radially, beyond the inner edge of the focal plane mask) was limited to $\sim 10^{-5}$ in that zone. In § 8 of this report we discuss our understanding of that limiting factor as a result of detailed modeling of the system as informed by the vacuum test results.

In addition to the milestone metric, a key goal of the investigation, *now successfully met*, was to mature and demonstrate the operability of the integrated EXCEDE test bench starlight suppression system, using key flight-like components (in particular the BMC MEMS DM), in a relevant ($\approx 3 \times 10^{-6}$ Torr, simulated low Earth orbit) vacuum environment. (I.e., closely approaching TRL 5⁶, with a current, predicted mitigatable, lien on IWZ performance.)

⁴ See § 4.4.4 and Figure 7 of JPL D-94365, but extended to $11 \lambda/D$ for the MS #2 demonstration.

⁵ For MS #1 we established an outer working angle (OWA) benchmark limited to a $4 \lambda/D$ configuration for our (now monochromatically demonstrated) in-air testing to allow for timely maturation using then existing, compatible, coronagraphic optics. For MS #2, we subsequently reconfigured the test bench with (in particular) new focal plane occulters and with existing inverse PIAA optics that, together, allowed exploration to an OWA of $< \sim 12 \lambda/D$, advantageously closer to the larger proposed final, flight DM limited, configuration.

⁶ http://www.nasa.gov/pdf/458490main_TRL_Definitions.pdf

3. Laboratory Configuration

3.1. Overview

This laboratory investigation/milestone demonstration was carried out in a vacuum chamber facility at the Lockheed Martin Advanced Technology Center. The EXCEDE vacuum compatible test bed was configured incrementally to its final demonstration form over five epochs of testing in the vacuum chamber with the goals of each vacuum chamber test (VCT) summarized in Table 1. The milestone demonstration was the part of the fifth and final VCT. The corresponding results and their modeling and analytic interpretation are discussed in detail in § 8 & § 9 of this report.

For the MS #2 investigation, the EXCEDE in-air test bed was modified from its initial layout as tested prior at the NASA Ames Coronagraph Experiment (ACE) laboratory [Sch13] to more closely approach the proposed flight instrument architecture. The primary considerations for this reconfiguration were the following:

- (a) Enabling an exploration/demonstration of contrast performance with polychromatic light with up to a 10% bandwidth vs. monochromatic light (650 nm was selected).
- (b) Verification of a wider outer working zone, with the final verification of the outer working angle set to $11 \lambda/D$ vs. $4 \lambda/D$.
- (c) Demonstration of system operability in a vacuum environment vs. ambient air.

In practical terms, the main laboratory updates as a result of these considerations were the:

- (i) usage of a supercontinuum white laser source with a selectable bandwidth filter
- (ii) introduction of inverse PIAA optics to enable a wider field of view with an unaberrated point spread function (PSF) in the final focal plane [Guy05]
- (iii) reconfiguration of the DM position to upstream of forward PIAA optics, to work in conjunction with the inverse PIAA system and to enable removal of tip/tilt modes (sensed by a LOWFS) prior to propagation through the forward PIAA system
- (iv) preparation of electronic components and optical mounts for the test bed for vacuum compatibility

3.2. Vacuum Chamber and Test Bed Facility

The vacuum chamber at Lockheed Martin is operated in a class 10,000 clean room. There is a large, vibration-isolated optical table inside the chamber on which the EXCEDE test bed is mounted. The entrance to the chamber and the final configured test bed are shown in Figure 1 (left), and views of the test bed within in Figs. 1 (right) – 3.

The test bed features no enclosure, as the intent is to operate in vacuum. This makes the test bed easier to access and align in air. This also implies, however, that high-contrast cannot be realistically achieved in air due to an uncontrolled environment. In vacuum, thermal gradients are monitored and mapped with temperature probes located on important components throughout the test bed, and the cameras cooled and outfitted with heat-sinks.

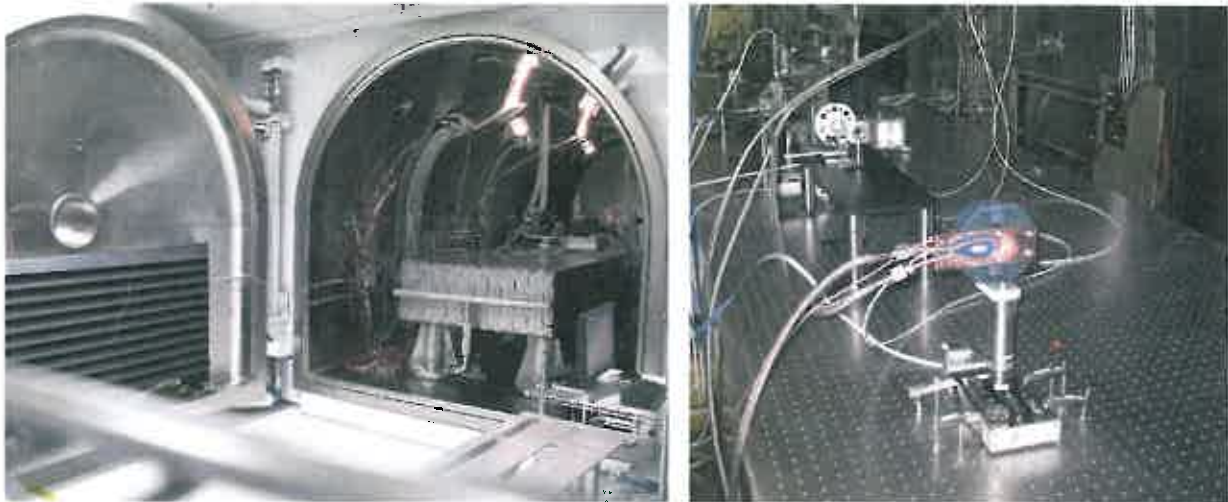


Fig. 1. Second milestone demonstration was performed in the vacuum MET chamber facility at Lockheed Martin Advanced Technology center. Left: Class 10,000 clean room at the entrance of the vacuum chamber. Right: View of the EXCEDE test bed from the science camera end.

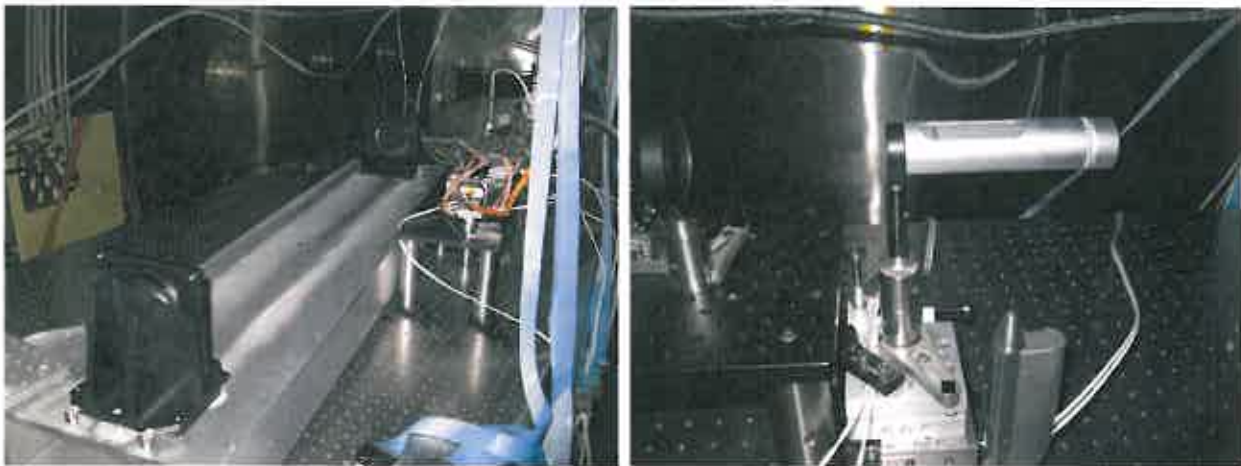


Fig. 2. Left: View of forward PIAA mirrors. Right: View of inverse PIAA lenses.

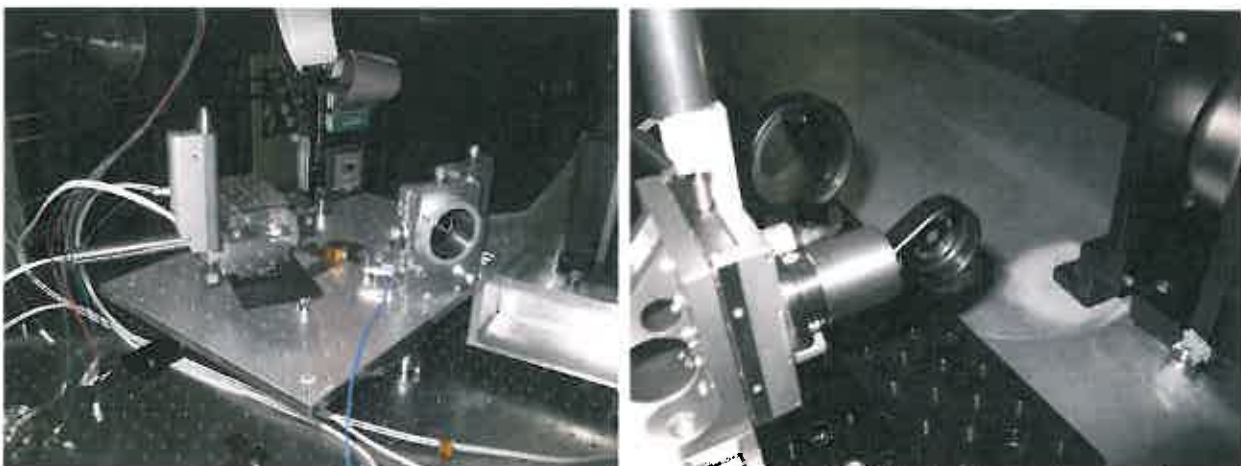


Fig. 3. Left: Front-end optics on platform with two OAPs and the DM. Right: Focal plane mask.

3.3. Optical Configuration

The final optical configuration of the EXCEDE test bed for the second milestone demonstration is shown schematically in Figure 4. The propagation of the beam from the external source stimulus to the science camera imaging detector at the final focal plane is described below.

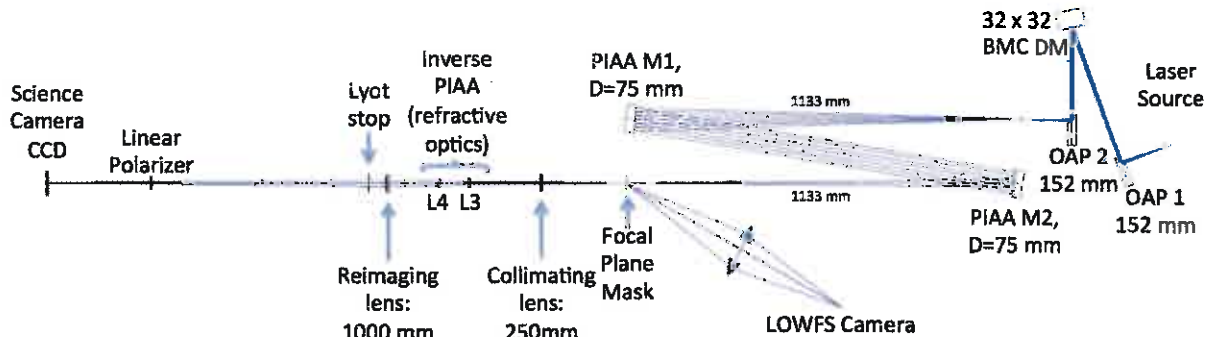


Fig. 4: Optical configuration of the EXCEDE test bed for the second milestone demonstration.

LIGHT SOURCES/INPUT FIBER: The light sources available for our test bed were several lasers, including a long-coherence-length 650 nm laser (Newport SWL-7505 which was baselined for monochromatic testing), a green HeNe or a diode laser at 532nm (for set up and alignments, but not used for the MS #2 demonstration), and a supercontinuum light source (an NKT photonics SuperK laser), coupled into a single mode fiber with a variable bandwidth filter (the SuperK VARIA tunable single line filter). As in the MS #1 demonstration, we used a single-mode fiber output as a reasonable approximation to a point-source (stellar) image delivered by a telescope. This fiber is fed into the vacuum chamber via a port hole.

The supercontinuum light source was used for the milestone runs in VCT #5, whereas the other sources were also used for earlier alignment and verification activities. To mitigate potentially deleterious chromatic effects in broadband light, reflective, rather than refractive optics were used both when necessary and whenever possible (notably, inverse PIAA optics used in this investigation were, within chromatic tolerance, refractive lenses).

OAPs: The laser source feeds front-end optics containing the DM that, as reconfigured for MS #2, was positioned upstream of the forward (two mirror) PIAA system, as proposed for the flight architecture. The front-end optics are shown in Figure 3 (left). Two OAPs, with $\lambda/4$ surface quality, are used for two main purposes: (a) to create a point focus input to the forward PIAA with an $f/15$ beam, and (b) to conjugate the DM with respect to the first forward PIAA mirror (M1).

DEFORMABLE MIRROR⁷: The DM used is a 32x32 actuator Boston Micromachines MEMS. The DM is conjugated to PIAA M1 to avoid geometrical distortion effects due to the

⁷ The DM used in VCT 1-4 suffered a catastrophic failure after the completion of VCT #4, discovered during in-air preparation work for VCT #5. Following a failure investigation, with the unit returned to BMC for independent evaluation, the cause was determined to be due to an operations error, and not any defect in materials,

forward PIAA system and to allow for wide field correction. The DM converts commanded voltages into displacement of individual actuators. The calibration procedure for the DM is described in detail in § 5.1.

FORWARD PIAA MIRRORS: The beam next propagates to the forward PIAA mirrors shown in Figure 2 (left). For cost containment with experimental sufficiency, we used the same generation-1 PIAA mirrors as in the first milestone demonstration. These mirrors are *not specifically optimized for broadband performance*. This, in part, limits the explorable bandwidth to $\leq 10\%$.

FOCAL PLANE MASK: The focal plane mask, shown in Figure 3 (left) is at the prime focus of the forward PIAA system. The focal plane mask has a C-shape deposit on glass with a reflective circular inner occulter blocking the core of the PSF. The light reflected from the inner circular occulter feeds to the Low Order Wavefront Sensor (LOWFS). A straight edge blocks one entire side of the focal-plane, and an outer circle blocks light at off-axis angles $> 16 \lambda/D$.

During the course of our incremental broadband system maturation, we replaced the FPM twice (see Table 1). First, with one adding an anti-reflection (AR) coating application to mitigate earlier seen optical ghosting. This FPM (used in VCT #4) also added a central opaque "dot" to remove on-axis photons from the LOWFS, and to help establish the system metrology on this larger than prior OWA mask. Second, with a higher optical depth coating of OD 6 for deeper PSF extinction in the partially transmissive central zone, and to adjust the size of the FPM that was originally optimized for the in-air test bed at the ACE laboratory. The final C-shaped FPM installed and used for VCT #5 (with the central dot removed) had an oversized IWA of $1.6 \lambda/D$, and OWA of $16 \lambda/D$. The position of the mask was offset so its interior edge along the axis of symmetry into the "dark hole" was $1.2 \lambda/D$ from optical axis (center of the PSF).

LOWFS: The central core of the PSF is reflected by the focal plane mask to the LOWFS system to measure pre-PIAA tip/tilt modes. A re-imaging lens is used to form a slightly defocused image on the LOWFS camera. A 14-bit ImperX Bobcat ICL-B0620 CCD camera provides a high frame rate and a National Instruments PXI controller establishes a real-time control loop with the DM. The design, performance, and operation of the EXCEDE test bed LOWFS is detailed in [Loz13, Loz14].

INVERSE PIAA LENSES: The inverse PIAA lenses are shown in Figure 2 (right panel) and are placed in a collimated space in order to reduce refractive effects in polychromatic light. As these lenses are located after the FPM, their aberrations do not impact the ability of the FPM to suppress the on-axis light.

workmanship, or other problem inherent in the unit. Upon completion of VCT #4 testing, voltage to the DM actuators should have been removed while (prior to) transitioning from vacuum back to air, but was not. This was fully documented in a NASA/ARC incident report. Subsequently, both procedural and H/W protection steps were taken to assure against a future similar occurrence. A replacement "plug compatible" DM unit was obtained from BMC and, with calibration and functionality/operability testing, was then used for all VCT # 5 testing without any impacts (other than schedule lost) to technical performance.

LYOT STOP: A Lyot stop is placed shortly after a final re-imaging lens, and thus in nearly collimated space. This defines the exit pupil and blocks out the edges of the second pupil plane diffracted light.

LINEAR POLARIZER: A linear polarizer located immediately prior to the science camera mitigates any instrumental polarization effects due to reflective optics in the system.

SCIENCE CAMERA: The science camera, located in a re-imaged focal plane after the linear polarizer, is used both for target imaging, and for closed loop mid-spatial frequency wavefront sensing and control with the DM. It has an as-calibrated linear image scale of 5.5 pixels per $1 \lambda/D$. This 16-bit QSI 520i series CCD camera provides a low read-noise output. It has a regulated thermoelectric cooler which is maintained at 1°C to avoid ice crystal formation during operation⁸.

⁸ Other contaminant deposition was discovered on the interior surface of the CCD window (a few mm ahead of the final focal plane) during in-air preparatory activities preceding VCT #5. These were manifested as slightly afocal (diffractive) spots on the science camera images. (Mild) bake-out of the window-sealed detector unit assembly did not remove the contaminant. The CCD window was subsequently removed, cleaned per the manufacturer's specifications, and reinstalled. This largely, but not fully, mitigated the contaminant deposition. The residual contamination, e.g., as seen as very small nucleation spots in Figures 11 & 17 (right panel) of this report, was found: (a) inconsequential to the operation, fidelity, and robustness of the SN WF control algorithm, and (b) only marginally (or insignificantly) affecting median raw contrast measures. Due to exhausted schedule margins ahead of VCT #5, no further action was taken to remove the residual contamination given it was found non-impacting by its presence on the experimental contrast measures and results.

4. EXCEDE Vacuum Chamber Tests: Schedule and Goals

The EXCEDE test bench was matured, and tested, incrementally in five epochs over fifteen months, *in situ*, at the LM ATC's MET test chamber facility, as summarized in Table 1. In the first two epochs (Vacuum Chamber Test [VCT] ID's #1 & #2 in Table 1) with work focused on the test bench alignment, operability, functionality, and initial characterization, all testing was done in ambient air. This permitted ready, and timely, access to the experiment bench for manual iterative adjustment and reconfiguration during these early testing phases.

TABLE 1 – EXCEDE MS #2 MET CHAMBER TESTING, GOALS, OUTCOMES

VCT	Dates	Vacuum	Goals	Outcomes and Next Needs												
1	12/20/13 01/01/14	No	FRONT-END TEST: Check: Strehl ratio, Stability, Phase & amplitude aberrations, Characterization and alignment of the optical elements.	Finish Imperx camera preparation, Improve DM illumination												
2	01/22/14 02/01/14	No	SPECKLE NULLING (SN): Wavefront Control	Install new cooling system and temperature probes Install inverse PIAA optics												
3	02/24/14 03/10/14	Yes	1. MS #1 IN VACUUM WITH SN: 2. Preliminary Broadband Assessment with non-optimized FPM* Tests with the front end complete including lens to adjust the <i>f</i> ratio of the beam at the PIAA entrance. H/W test: Automatic liquid cooling for the cameras. *(7.2 λ /D IWA, shifted to 1.2 λ /D)	MS #1 in vacuum achieved INITIAL broadband contrast measures obtained at 2-6 λ /D and 2-12 λ /D. Next test: Change-out FPM (to #2): - proper IWA/OWA - AR coating (to mitigate ghosting) - central alignment "dot"												
4	08/11/14 10/20/14	Yes	IMPROVE CONTRAST PERFORMANCE: H/W Test: Vibration reduction with new camera cooling system Characterize replaced FPM (#2) Note: Using AR coated, 16 λ /D FPM	Best Interim Contrasts Achieved: <table border="1"> <thead> <tr> <th>bandwidth</th> <th>1.2-2 λ/D</th> <th>2-12λ/D</th> </tr> </thead> <tbody> <tr> <td>MONO</td> <td>8E-7</td> <td>6E-8</td> </tr> <tr> <td>1.5%</td> <td>8E-6</td> <td>2E-7</td> </tr> <tr> <td>10%</td> <td>3E-5</td> <td>3E-7</td> </tr> </tbody> </table> Next test: Need to change FPM (#3) for deeper center PSF extinction and remove central dot	bandwidth	1.2-2 λ /D	2-12 λ /D	MONO	8E-7	6E-8	1.5%	8E-6	2E-7	10%	3E-5	3E-7
bandwidth	1.2-2 λ /D	2-12 λ /D														
MONO	8E-7	6E-8														
1.5%	8E-6	2E-7														
10%	3E-5	3E-7														
<i>Change-out Post VCT #4 of Failed Deformable Mirror - see footnote 7</i>																
<i>Science Camera CCD Camera/Window Contamination Mitigation - see footnote 8</i>																
5	02/24/15 03/31/15	Yes	RIGOROUS PERFORMANCE CHARACTERIZATION and ACQUISITION OF CDP⁹ DATA: Repeatability and Stability Generation of CDP evaluation data	CDP Data Obtained. Results § 7. System modeling and simulations to understand broadband IWZ performance; § 8.												
<i>Early termination (3/28/2015) of VCT #5 due to facility power interruption/loss of vacuum - see footnote 13</i>																

⁹ Certification Data Package (CDP): experimental data per § 6.1.5 of JPL D-94365; algorithmic codes and data files delivered electronically are described in Appendix C.

5. EXCEDE MS #2 Vacuum Test Bed System Calibration

Details of, and processes planned for, the EXCEDE test bench key component, sub-system, and end-to-end system calibration are presented in JPL D-94365 [Sch15], § 4. Herein we elaborate on additional, or modified, procedures and calibrations that evolved from the needs of the experimental investigation beyond those discussed in earlier documents and publications.

5.1. Deformable Mirror Calibration

The BMC 32x32 actuator format deformable mirror (DM), used both for the prior reported milestone #1 demonstration (JPL D-81372) and for the first four (of five) vacuum environment test runs, was replaced (after unit failure; see footnote 8) prior to the final vacuum run demonstrating broadband contrast performance. The replacement DM (an identically manufactured unit from BMC) had to be calibrated anew to obtain an accurate deflection curve for its commanding, as well as a voltage map enabling an attainment of an initial surface with flatness better than $\lambda/20$ ¹⁰.

A first procedure, used to develop a model for the response of a representative DM actuator through a deflection curve, was as follows:

5.1.1. A Zygo interferometer was setup to measure the surface of the DM. This setup consisted only of the Zygo and the MEMS DM.

5.1.2. A set of voltages was applied identically to a representative set of three widely separated actuators ranging from 0V to 200V (from which an average response was estimated in 5.1.3).

5.1.3. For each voltage applied, the maximum surface stroke of each of the three DM actuators activated was measured, resulting in three deflection curves (see Fig. 5) that were reduced using a matlab routine included in the CDP (DM_deflection_ST.m). A separate consistency cross-check was conducted on a single actuator, reading the measurement directly from the Zygo GUI.

¹⁰ The BMC MEMS actuator influence functions, that were needed for our MS #1 demonstrations employing EFC WF control, were also measured (as discussed in JPL D-81327; see § 3.4.2 and footnote 8 of that report) for the replacement DM. However, these were not used with the SN WF control algorithm employed exclusively in our MS #2 demonstrations (§ see 6.1), and so we do not discuss them in this report. SN is done primarily in an iterative fashion without reliance on the influence function, whereas EFC is forward modeled using the influence function. As an additional detail (though not relevant for the conduction of the MS #2 experiment), in measuring the influence functions we scanned in phase and amplitude to determine which combination of both was giving the better contrast. (One can argue that it is a slower process, but it is more robust, e.g., against incoherent light).

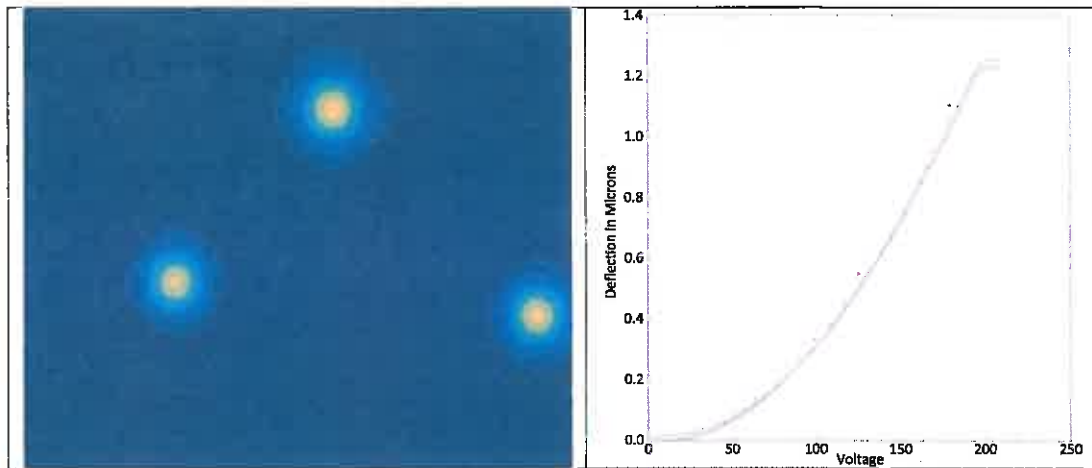


Fig. 5. Actuator pattern (left) and the results including the direct Zygo measurements (right).

The second, iterative, procedure used to obtain an initial flatness on the DM surface better than $\lambda/20$ was as follows:

5.1.4. A Zygo interferometer was setup in the same manner as 5.1.1 to measure the surface of the DM, with actuators set at a bias voltage (140V) as the initial assumed DM flat setting.

5.1.5. DM surface interferometric measurements were obtained with the Zygo.

Details: A first set of phase measurements was obtained using a pattern of selected poked actuators to estimate the scale of the Zygo wavefront map relative to the linear pitch of the DM actuators (i.e., the scale in pixels/actuators) and the orientation of the DM actuator grid relative to the bench. The pattern was as shown in Figure 6 with a linear DM scale of 3.43 pixels per actuator, and with a 90° rotation in image orientation and parity flip, that were included in the final Labview software built to control the DM.

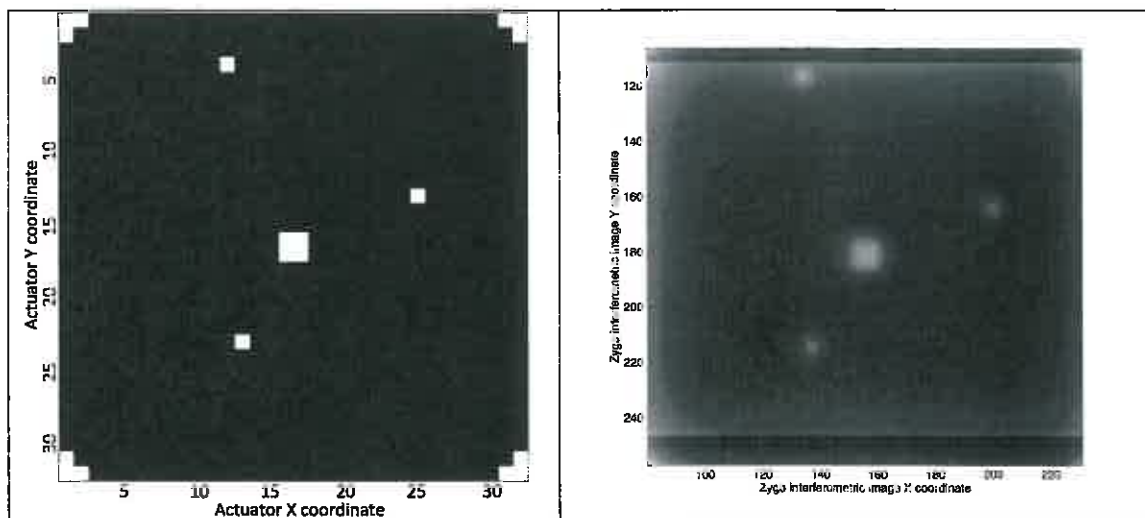


Fig. 6. Left: "Poked" DM actuators. Right: Zygo interferometric image (rotated and scaled to the geometrical frame of the DM) showing the "poked" actuators. (N.B.: On close examination one can also see the scalloping of all the MEMS actuators).

For calibration/reduction, a separate interferometric image is then obtained without the calibration pattern (poked actuators). With the orientation and the scale defined, the Zygo images were post-processed (bad pixels rejected/corrected, depistoned, detilted, and low-pass filtered as needed). The final image is of the residual wavefront error (in microns) due to the DM. The new DM actuator settings that correct the DM aberrations were then computed. The last step was then to use the deflection curve estimated in the first step of the DM characterization to derive the final voltages.

5.1.6. Repeat steps 5.1.4 – 5.1.5 until the DM flatness converges to $\leq \lambda/20$.

5.2. Input Fiber Alignment

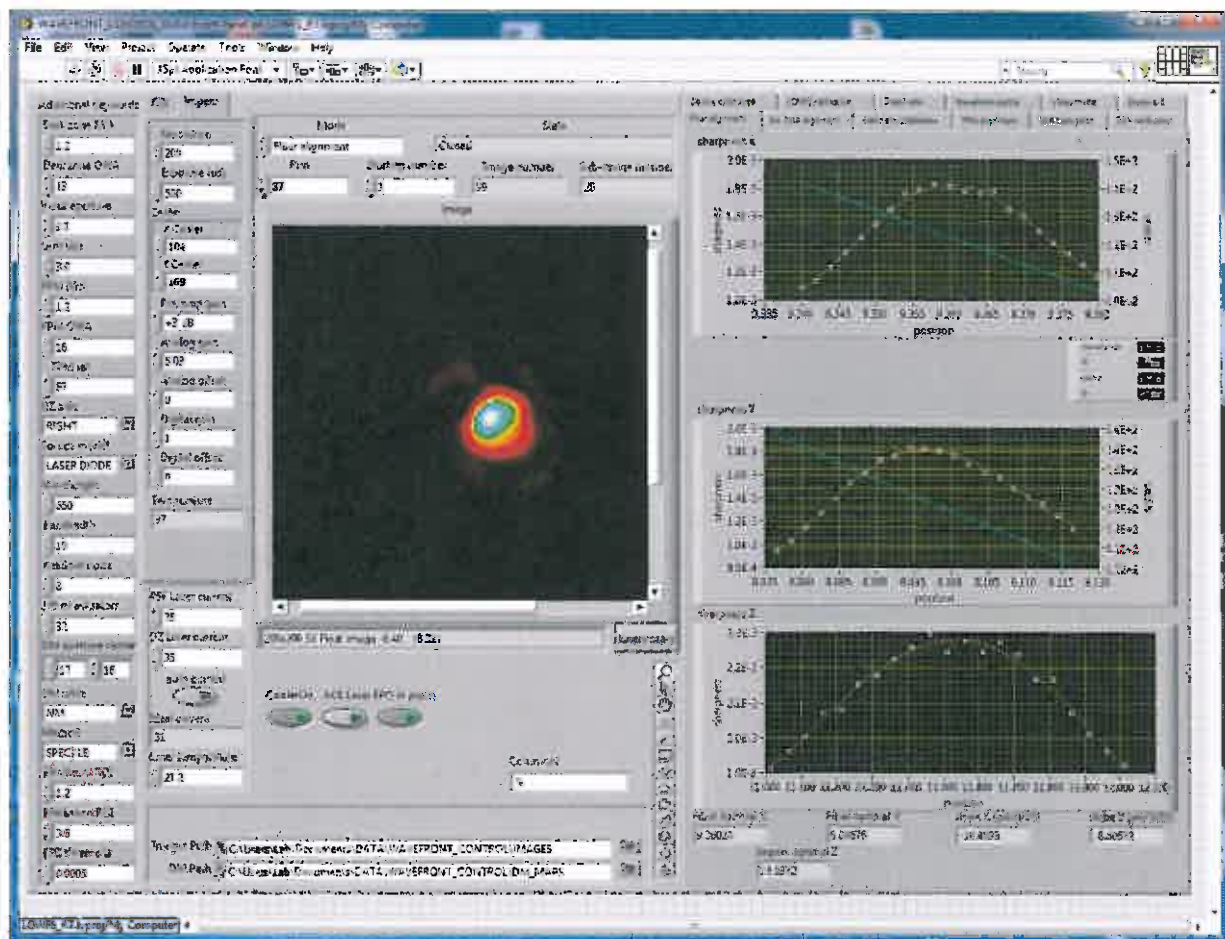


Fig. 7. Labview GUI for aligning the input fiber.

This procedure, the co-alignment of the input fiber source for the MS #2 demonstration, is as spoken to in § 3.4 (sub-section on Optical Alignments) item (1a) JPL D-94365 with modifications as described below. The input fiber was aligned in both orthogonal directions (X, Y) in the transverse plane with respect to the optical axis, to assure on-axis concentricity with respect to both the front-end optics, and to the PIAA system. The procedure adopted was different in detail from the fiber alignment procedure used for Milestone #1 demonstration. The change was due to the introduction of the inverse PIAA optics after which it was no longer

preferable to use the science camera for this alignment. Instead, the LOWFS camera was used, using light reflected from the focal plane occulter.

The iterative procedure adopted for aligning the input fiber was as follows:

5.2.1. The focal plane occulter was used to completely block the PSF on the science camera.

5.2.2. The fiber was first moved (on an XYZ translation stage; Z pre-set during manual alignments) along the X-axis of the transverse plane, with an optimization criterion for its position where the sharpness¹¹ metric of the image formed on the LOWFS camera was maximized.

5.2.3. The fiber was then moved, orthogonally, along the Y-axis of the transverse plane, with the same maximum sharpness criterion as 5.2.2 for its location optimization.

5.2.4. The LOWFS camera was then translated along the optical axis to determine the "best" in-focus location by maximizing the sharpness metric of the image formed on LOWFS camera.

5.2.5. Steps 5.2.2 – 5.2.4 were repeated until both the fiber and LOWFS camera locations were stable.

5.3 Inverse PIAA Alignment and Image Scale

For this demonstration, inverse PIAA optics (in the form of two lenses) were added to the optical configuration of the EXCEDE test bench (see JPL D-94365 Figure 5, Table 1, and § 3.2 for details). Following the input fiber alignment, the location of the inverse PIAA lens assembly was determined to assure on-axis concentricity with respect to the forward PIAA mirrors and other front-end optics. In addition, the best-focus location for the science camera was established, and the image scale in terms of pixels per λ/D at the science camera image plane was measured. This procedure was as follows:

5.3.1 The focal plane occulter was moved out of the optical path in order to assure the formation of a fully unocculted image of the inverse PIAA PSF on the science camera.

5.3.2. The inverse PIAA lens assembly was moved along the X-axis of the transverse plane, with an optimization criterion for its position where the sharpness metric of the image formed on the science camera was maximized.

5.3.3. The inverse PIAA lens assembly was moved, orthogonally, along the Y-axis of the transverse plane, with the same maximum sharpness criterion as 5.3.2 for its location optimization.

¹¹ "Sharpness" defined as $\sum \text{image}^2 / (\sum \text{image})^2$ over all pixels in a fixed size photometric aperture capturing all of the flux in the PSF core.

5.3.4. The science camera was moved along the direction of the optical axis to determine the best focus location by maximizing the sharpness metric of the image formed on the science camera. If the position scan (e.g., Fig. 8 top right curve) was decentered the previous alignment step were repeated.

5.3.5. The input fiber was moved along the X-axis of the transverse plane by a known amount and the image scale along this axis, in terms of pixels per λ/D at the final image plane, was measured as a function of the fiber translation distance.

5.3.6. The (X-recentered) input fiber was moved along the Y-axis of the transverse plane by a known amount and the image scale along this axis, in terms of pixels per λ/D at the final image plane, was measured as a function of the fiber translation distance.

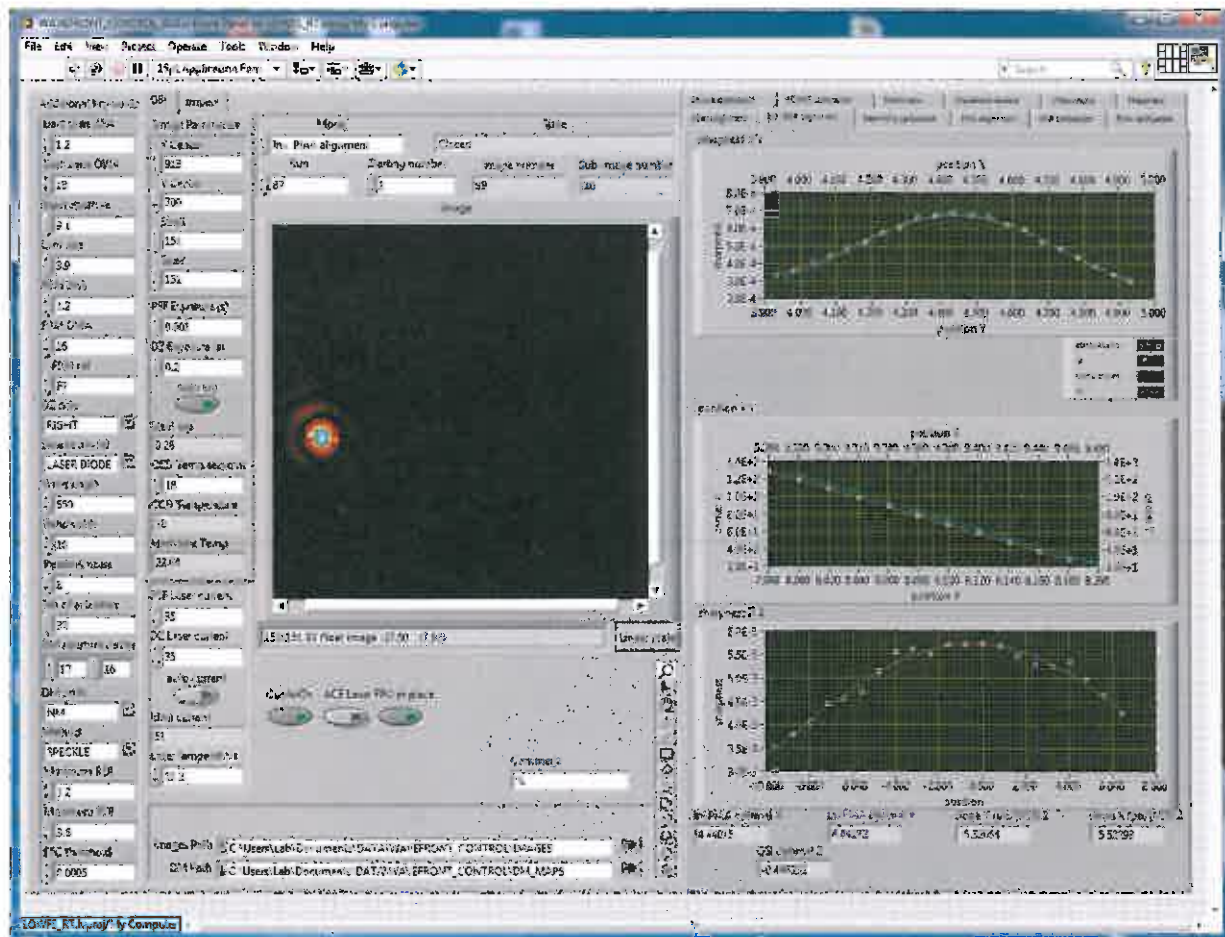


Fig. 8. Aligning the inverse PIAA lens assembly.

5.4. Contrast Calibration

An unoccluded reference image of the PSF of the aligned system must be obtained at the same central wavelength and band pass used during wavefront control to enable contrast calibration.

In the EXCEDE test bench setup for "narrow" bandwidths, $< 10 \text{ nm}$ ($\approx 1.5\% @ 650 \text{ nm}$), to obtain such a reference image:

5.4.1a. The focal plane occulter is moved to allow the PSF to pass through a transparent part of the mask, so an unocculted image of the PIAA PSF is formed on the science camera.

5.4.2a. The flux density in every pixel in the image of the core-occulted PSF is measured, and then is divided by the flux density in the central (peak) pixel in an unocculted image of the PSF; this ratio gives the dimensionless stellocentric contrast of every image pixel.

This image also serves to accurately identify the center of the PSF in defining the stellocentric dark zone. Further characterization of the PSF that gives (as above) the position of the on-axis PSF, the rotation angle between the DM and the science camera, and the focal plane scale is ascertained per steps 4.4.2 – 4.4.4 of JPL D-94365.

For spectral bandwidths > 10 nm, image saturation in the science camera occurs at the shortest possible currently available exposure times. In these broadband cases, we measure the ratio of the flux density of monochromatic/narrow and polychromatic/broad PSFs from the reflected light on the focal plane occulter using the LOWFS camera. The measurements are as follows:

5.4.1b. The focal plane occulter mask is moved to: (1) completely block all light from the PSF, and (2) ensure all the stellar the energy is reflected from the focal plane mask to the LOWFS.

5.4.2b. The source intensity on the LOWFS camera is integrated for the ≤ 10 nm case.

5.4.3c. The source spectrum is extended to the wider desired spectral bandwidth.

5.4.4d. The source intensity on the LOWFS camera is integrated for the broadband case.

5.4.5b. The source intensity ratio of the broadband to the narrow PSFs are directly computed. This ratio is used when computing the intensity of broadband contrast field by adjusting the peak flux density by the appropriate contrast calibration by this factor (augmentation to 4.4.5 in D-94365.)

N.B.: Details of the source calibration to obtain image contrast using the LOWFS are provided in Appendix B of this document.

5.5. Focal Plane Mask Alignment and Inner Working Angle Verification

The following calibration procedure was employed to assure that the C-shaped focal plane occulting mask was correctly aligned and positioned.

5.5.1. The focal plane occulter mask was moved first in the same transverse direction as the C-shaped mask's straight edge. At each location the total energy in the image obtained was summed, and divided with respect to the energy in the unocculted PSF, i.e., to obtain the relative fractional energy recorded. The occulter location along this axis of motion was chosen to minimize the relative energy.

5.5.2. The focal plane occulter mask was moved along the second (orthogonal) transverse direction, perpendicular to the C-shaped mask's straight edge. The relative energy was computed at each measured location in the same manner as 5.5.1. The occulter location along

this axis was chosen such that the relative energy was 50%. (For the EXCEDE/PIAA system, the IWA is defined where the coronagraphic throughput is 50%.)

A second procedure (5.5.3) was used to verify at any time the location of the C-shaped occulter without necessity of re-alignment of the occulter:

5.5.3. The fiber was displaced along the transverse direction perpendicular to the C-shaped mask's straight edge. The location of the IWA (50% throughput) was measured. The goal was to assure that at any time (and, in particular at the end of a wavefront control iteration), the IWA remained stable at a desired $1.2 \lambda/D$. This process assures that the PSF was not moved by tilts introduced on the DM by the wavefront control algorithm, and that no other changes in the system affected the location of the IWA. The verification procedure has $\pm 0.05 \lambda/D$ uncertainty.

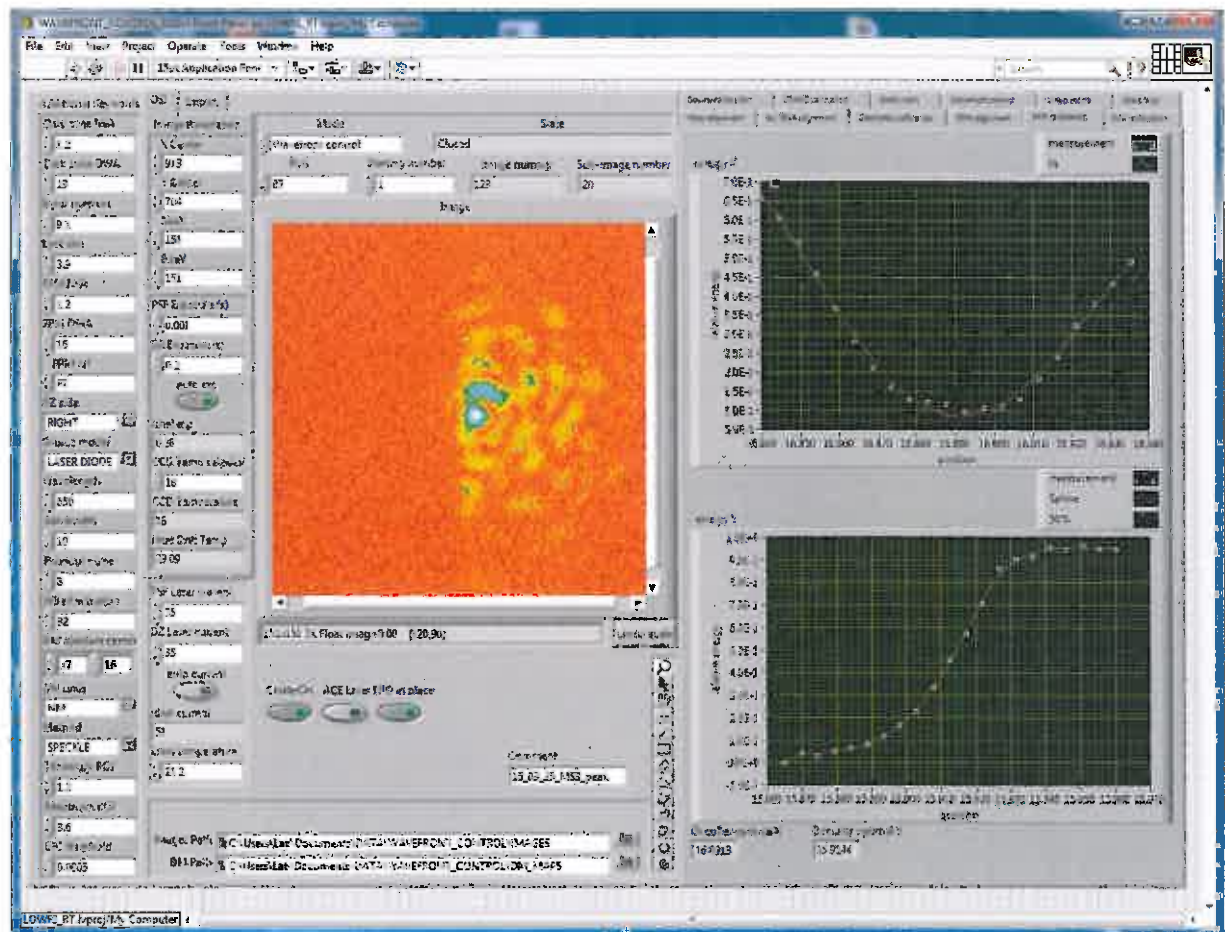


Fig. 9. Aligning the focal plane mask.

5.6. Low Order Wavefront Sensor (LOWFS) Calibration

The LOWFS corrects the pre-PIAA tip and tilt modes. The LOWFS uses reflected light from the focal plane mask. The core of the reflected PSF from the circular inner part of the C-shape mask is focused onto a high frame-rate camera with a slight defocus. Using only a (sufficiently large) 50×50 pixel sub-array in the central part of the camera allows frame-rates higher than

1kHz. A real-time controller is used to collect images, decompose the images into tip/tilt modes, and send actuations to the DM to close a loop on the tip/tilt disturbance.

The LOWFS calibration procedure is as follows:

5.6.1. A reference image of the reflected PSF is constructed by collecting an initial set of images from the LOWFS camera. Subsequent measurement images are subtracted with respect to the reference image and the shifted centroid is computed.

5.6.2. A known set of tip/tilt modes are applied on the DM to construct an influence matrix with respect to the LOWFS focal plane.

5.6.3. As a one-time procedure for the system, the input fiber is displaced a known amount ranging from -1 to $1 \lambda/D$ individually for each tip and tilt axis to obtain a unit conversion between LOWFS focal plane pixels and system tip/tilt in λ/D .

N.B.: Separately, see Appendix B for using the LOWFS to calibrate the (relative) source intensity.

6. Milestone #2 Demonstration

6.1. Milestone Procedure

With the specific exceptions noted below, primarily in regard to wavefront control, the test, calibration, and data acquisition processes carried out in VCT #5 leading to the development of the CDP data sets (described in Appendix C) followed the Milestone #1 procedure as set forth in § 4.1 of JPL D- 81372.

For the MS #2 mid-spatial frequency wavefront control, we used our speckle nulling (SN) algorithm exclusively (rather than alternately, or additionally, EFC). This decision was predicated primarily by test schedule constraints and the state of "turn key" maturity of the operating S/W, rather than any expectation of performance differences once the WFC algorithms converge (e.g., see § 8.4.3). Our SN S/W was developed in LabView, with a graphical user interface as shown in Figure 10.

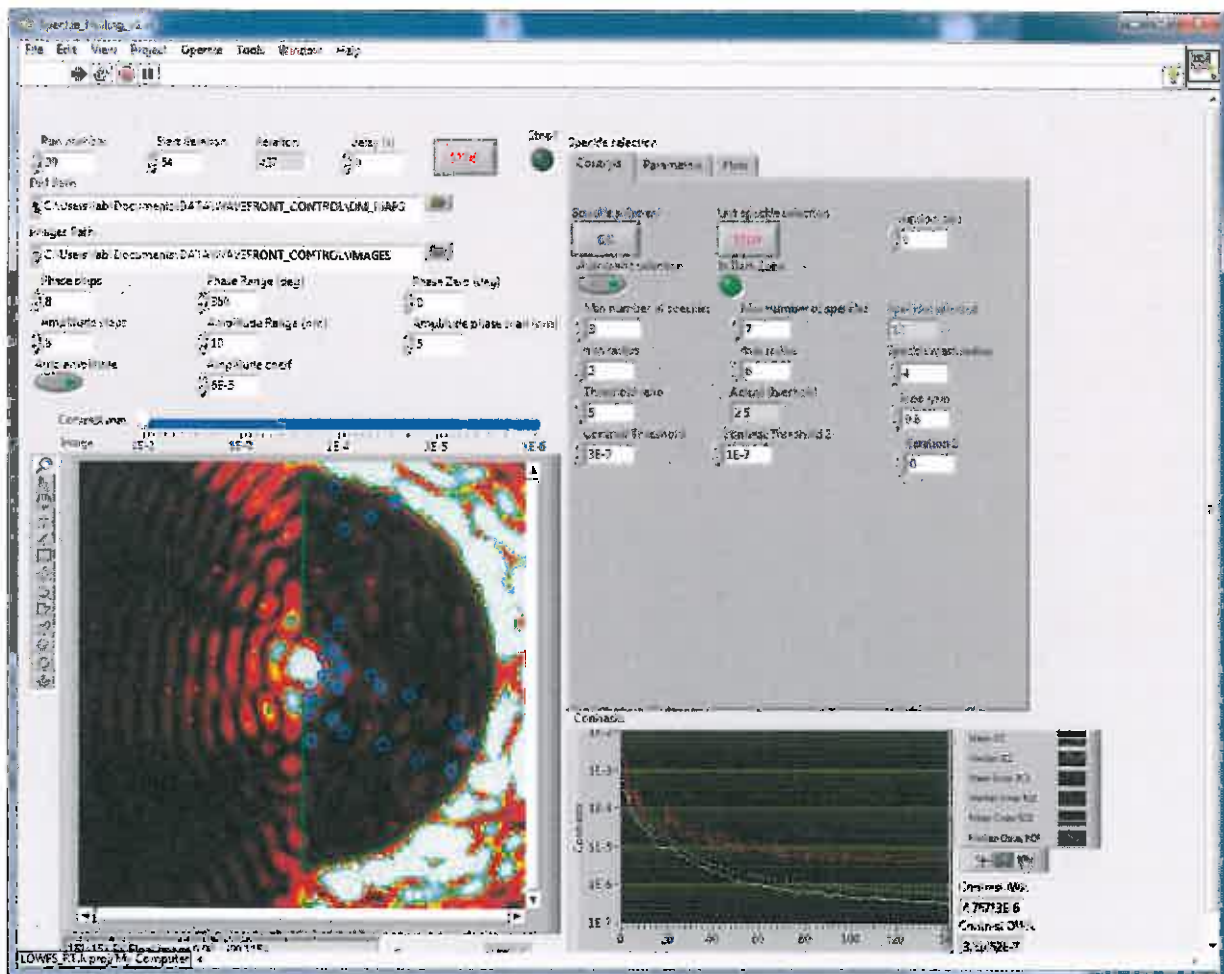


Fig. 10. Speckle Nulling Wavefront Control S/W User Interface

The process was as follows:

- 6.1.1 Calibrate the system, as per §§ 5.2 – 5.4 with the supercontinuum light source at 650 nm wavelength and 10 nm bandwidth.
- 6.1.2 With the OWA set to $12 \lambda/D$, start SN without the LOWFS.
- 6.1.3 Run the iterative SN algorithm until the system reaches about 10^{-6} contrast in the OWZ, and close to 10^{-5} in the IWZ.
- 6.1.4 When the above contrasts are attained, stop the SN control loop and recalibrate the focal plane mask position per § 5.5 of this document.
- 6.1.5 The LOWFS is then calibrated per § 5.6 with the new PSF position and shape before starting the active correction.
- 6.1.6 Start SN again to achieve high contrast and with parametric adjustment to the algorithm to approach the milestone.
- 6.1.7 Take ≥ 1000 images without any WF control algorithm actively running (this is equivalent to having WF algorithm running with a loop gain of zero)¹².

6.2. Milestone #2 Data Collection

Instantaneous measurements of the coronagraphic contrast field, per section 4.4 of JPL Document D-75787 (but in 4.4.2b extended for MS #2 to $11 \lambda/D$), were collected during VCT #5 to assess the end-to-end broadband contrast performance of the EXCEDE starlight suppression system test bench.

These measures were derived from data acquired with the EXCEDE vacuum test bed science camera, during the interval 23 – 28 March 2015¹³, in independent trial “runs” of ≥ 1000 continuous measurements after resetting the DM to scratch and newly re-establishing a wavefront corrected dark hole for each run by speckle nulling.

Data sets resulting from each trial run, as defined in step 4.6.5 of the JPL Document D-94365, were produced and archived from these raw and calibrated images. After initial experiments with the hardware and wavefront control software in the VCT #5 configuration, the system was producing stable and reproducible results amenable to analysis, modeling, and performance evaluation.

¹² This is what we expect in a flight mission, with an adaptive gain going to zero after the wavefront control algorithm has converged and is stable.

¹³ N.B.: A facility power loss at the LM/ATC campus caused a spontaneous loss of vacuum on March 28, 2015, during the planned period of CDP data collections (3 days before the scheduled completion of VCT #5). Recovery of the remainder of the planned test timeline was not possible due to the, then, subsequent unavailability of the MET chamber facility. Fortunately, sufficient data were collected by the time of the shut-down to proceed with a full analysis of the test results even though the broadband IWZ contrast goal had not yet been met.

7. Milestone #2 Results

In compliance with data acquisition criteria 5.1 = 5.4 in JPL D-94365, here in Figure 11, and as delivered with the originating data in the milestone #2 CDP, we present stellocentric fields obtained in three independent speckle nulling wavefront control runs to establish the "dark zone" with the EXCEDE PIAA coronagraphy test bed at 650 nm and 10% bandwidth.

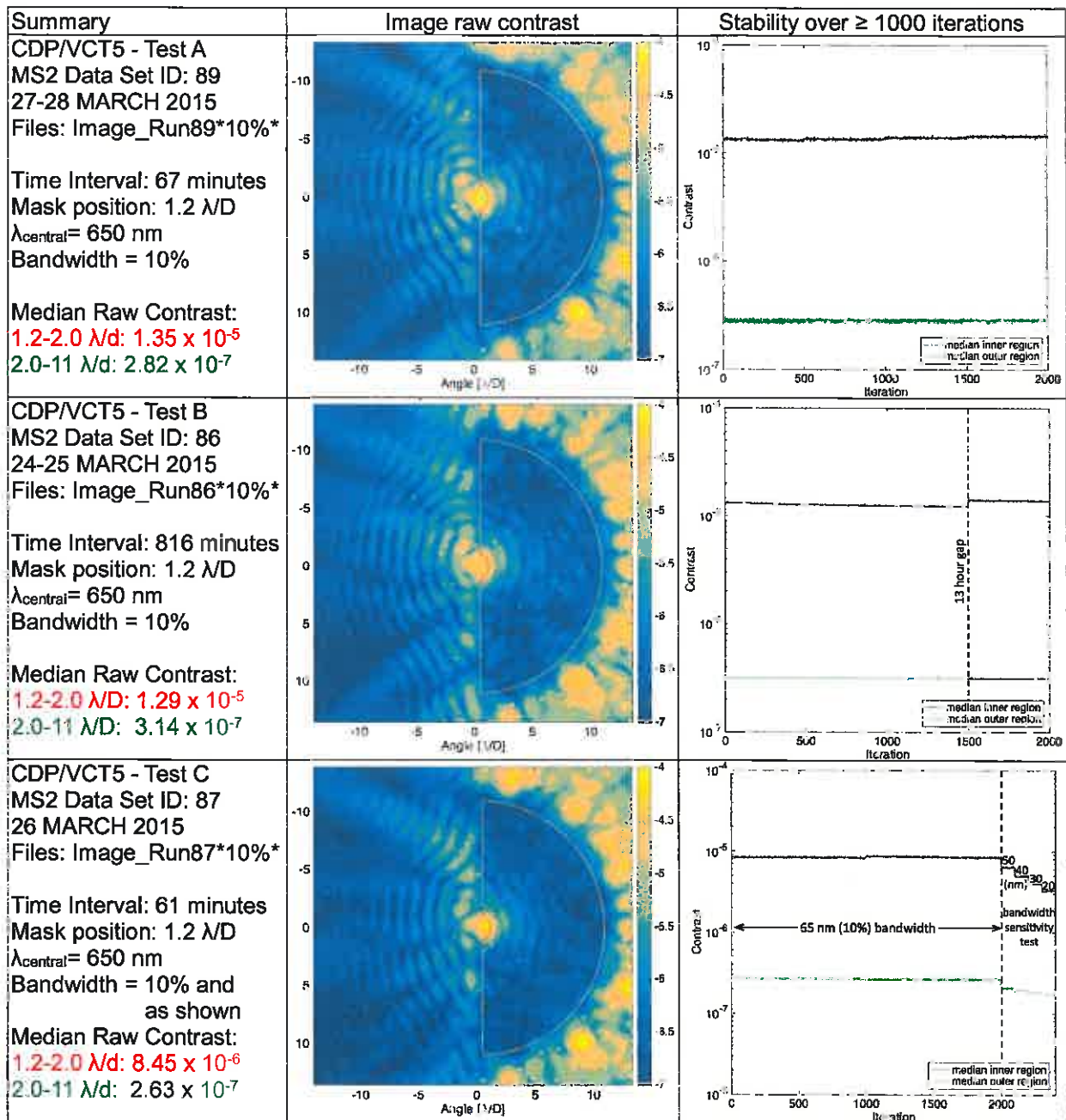


Fig 11. Demonstration of 10% bandwidth starlight-suppression: 1.2 – 11 λ/D @ 650 nm.

In the left panels, we tabulate the OWZ and IWZ median raw contrasts obtained averaging over all continuous iterations in each of the independent three runs. *In all cases, the OWZ contrast goal of $\leq 3 \times 10^{-7}$ was repeatedly met* (to the single digit level of precision for which the goal was established; see graphs in column 3). Averaging the three independent OWZ results gives $2.9 \pm 0.2 \times 10^{-7}$ raw median contrast over 97.9% of the dark hole area. Within the 0.8 resels beyond the inner edge of the $1.2 \lambda/D$ stellocentric focal plane mask, i.e. *in the $1.2 - 2.0 \lambda/D$ semi-annulus, the simultaneously raw median contrast goal of 10^{-6} was not met*, but fell short with a repeatable median raw contrast of $1.2 \pm 0.3 \times 10^{-5}$. We model, and discuss, this order-of-magnitude shortcoming with respect to the MS #2 IWZ metric in § 8 of this report leading to an understanding of the limiting factors as demonstrably mitigatable in a future test.

For each of the three test runs characterized in Figure 11, a single, but typically representative, contrast field image (from the ≥ 1000 obtained) is shown. The individual images (available as FITS files in the CDP) are highly repeatable, as evidenced in the contrast stability plots for each test presenting the raw median contrast metric as a function of image iteration.

In all three cases, data were collected with the establishment of the dark zone by SN for ≥ 1000 iterations, as follows:

In test A (top panels), 2,000 images were collected contiguously using 0.05s duration exposures with a time-averaged cadence of one frame every 2 seconds (over 67 minutes).

In test B (middle panels), we took the opportunity to test the longer term stability of SN by continuously taking data over ~ 14 hrs¹⁴. We began with 1,500 images collected similarly to test A (but with 0.25s exposure time). Then, without resetting the DM, we explored broadband performance at other bandwidths (from 50 nm to 10 nm, not illustrated here, but spoken to in § 8.4.2) for ~ 13 hrs, before contiguously collecting another 500 images at 65 nm (10% bandwidth). The stability of the SN-established WF control over that period of time is evidenced by the contrast metrics at 10% bandwidth that are graphed (collapsed across the 13-hour "gap" when data were being taken at other bandwidths) in Figure 11 (right panel). No change in OWZ contrast is seen (and no significant changes in image structures appear, if individually examined), over this longer period of time. A small degradation in the IWZ contrast is seen, however, at \sim the 15% level (though, as noted prior, is off the mark w.r.t. the milestone #2 IWZ metric).

Test C (bottom panels) was executed similarly to test B, but with 2,000 65nm (10%) bandwidth samples taken at shorter exposure times (1000 images at with 0.1 s exposures, followed by another 1000 iterations with 0.14 s exposures). We use those 2,000 images for our 10% bandwidth contrast metrics. Following that, as in test B, the bandwidth was incrementally decreased in consecutive iterations, in this case, of 100 images each that are shown here for information only¹⁵. The 65 nm (10%) bandwidth results are virtually identical to tests A and B in the OWZ. In the IWZ the contrast is improved by $\sim 37\%$ relative to test A, but remains about a factor of 8 above the milestone #2 IWZ contrast goal.

¹⁴ This timescale corresponds to $\sim 6x$ the orbital timescale for the proposed EXCEDE flight mission's 2000 km low-earth circular orbit.

¹⁵ As illustrated by the improvements in contrast with decreasing bandwidth, the level of SN-established wavefront correction is robust against changes in the spectral bandwidth over this range.

8. Model Comparison

To better understand the physical limitations of the as-implemented test bed, and in particular to identify the factor(s) limiting the experimental performance informed by the VCT #5 test results, specifically at the smallest stellocentric angle in the Inner Working Zone between 1.2 and 2.0 λ/D , we provide here in detail a description of, and the results from a performance sensitivity analysis.

8.1. Model Description

We have adopted a relatively simple optical propagation model with all the optical planes in the system modeled defined as Fourier conjugates. Despite its relative simplicity, the model replicates the observed performance (and limitations) of the experiment quite well (as we will demonstrate). This model of the EXCEDE test bed coronagraphic optics is schematically illustrated at a high level in Figure 12.

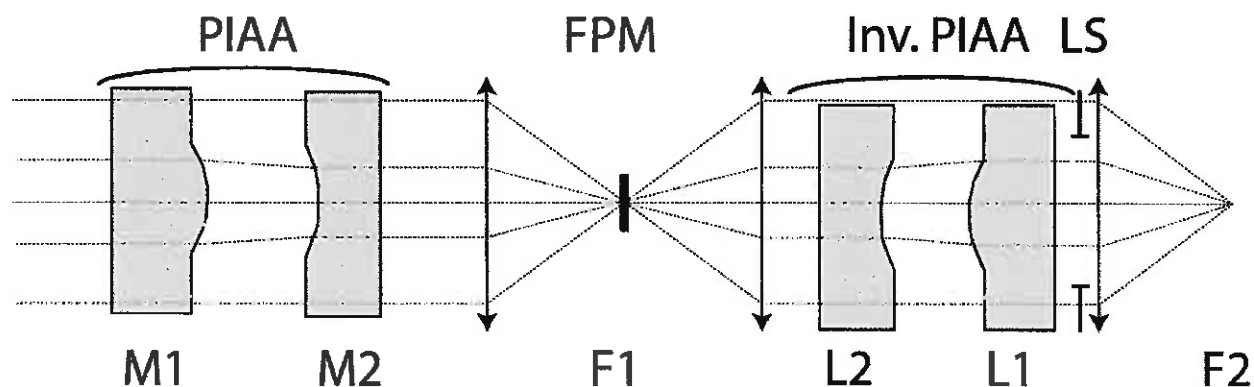


Fig. 12: Optical element and plane definitions for the optical model employed. The forward PIAA consists of the two mirrors M1 and M2 (illustrated only for simplicity as transmissive optics). The Focal Plane Mask (FPM) is located at the first focal plane F1. The Inverse PIAA consists of two inverse lenses L2 and L1. A Lyot stop (LS) is located at the exit pupil, and the final science image is formed at the re-imaged focal plane F2 (see Figure 4 for the complete optical layout).

The EXCEDE layout contains forward PIAA coronagraphic optics with two mirrors. These mirrors are defined by two planes at M1 and M2. The propagation between M1 and M2 is defined in our model by a ray-tracing pupil-mapping function. The intensity at the forward PIAA exit pupil (M2) is shown in Figure 13 (left). The DM is physically located upstream of the PIAA system and in the simulation this is approximated as the DM being conjugate to M1.

The C-shaped Focal Plane Mask (FPM) as shown in Figure 13 (right), is located at the first focal plane F1. The propagation between the exit PIAA pupil at M2 and the entrance pupil of the first inverse PIAA lens at L2 is performed using a convolution operation (with a Fourier transformation of the FPM).

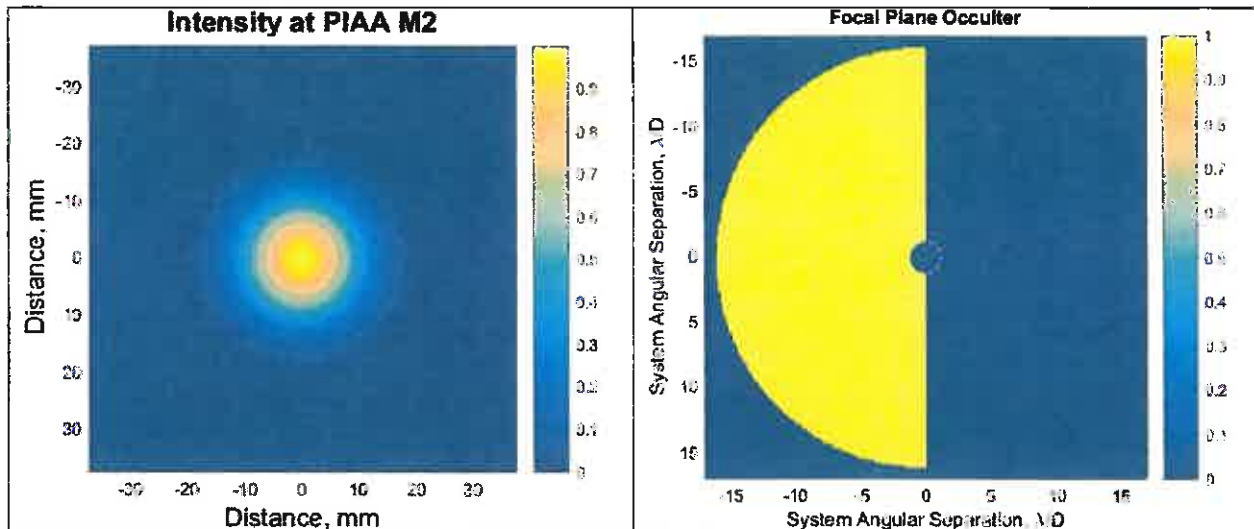


Fig. 13: Left – Intensity at the PIAA exit pupil M2. Right – C-shaped Focal Plane Mask with OD 6 partially transmissive inner circular occulter (within dashed circle).

The inverse PIAA lenses at L2 and L1 perform an inverse pupil-remapping operation to the forward PIAA mirrors also modeled through ray-tracing. At the exit pupil of the inverse PIAA system, a Lyot stop blocks diffracted light from the focal plane mask. The physical dimension of the PIAA system, the corresponding magnification and sizing of the focal plane mask, the open diameter of the Lyot stop, and the pixel sampling at the final science plane are all matched to the experimental test bed; See Table 1 of JPL D-94365 for a optical component overview corresponding to the layout in Figure 4 of this report.

All optical aberrations are collocated at the entrance pupil of the system, the M1 plane, and are propagated through the system as described. These aberrations can be corrected with the DM using either the iterative Electric Field Conjugation (EFC) or Speckle Nulling (SN) wavefront control algorithms. As in the VCT #5 demonstration, the WF corrections are applied for the central wavelength of 650 nm, the DM setting is maintained, and the input light bandwidth is extended to $\Delta\lambda/\lambda_{\text{central}} = 10\%$. This procedure follows the experimental correction.

Experimentally, SN was used exclusively for the MS #2 demonstration in VCT #5. Because we are interested in understanding the ultimate effect on the image contrast due to physical limitations of the test bed, perfect knowledge of the system model is assumed. An implicit assumption made here is that the wavefront control algorithm itself is not a limiting factor; see § 8.3.4.

8.2. Ideal Performance

To establish a baseline against which to compare the observed limitations of the experiment in VCT #5, we simulate the performance of the system first under ideal conditions with SN. This involves generating only a pure $\lambda/20$ phase aberration with a decreasing frequency ramp ($1/f^{3/2}$) in amplitude and assuming the circular occulter of the focal plane mask is completely opaque. In this idealized case, the starting contrast in the dark hole region is limited only by speckles caused by relatively high frequency scattering giving rise to a PSF with a near-unity Strehl ratio of 0.99. The result of this ideal case for 10% broadband light (without low-order aberrations; see

§ 8.3) is shown in Figure 14. Thus, we conclude that the EXCEDE starlight suppression system as configured for VCT #5, under ideal conditions, would fall short of the 10% bandwidth IWZ milestone metric by a factor of ~ 2 . A pre-test lower fidelity model, improved upon here (see Appendix D), predicted reaching the MS#2 IWZ contrast in 10% broadband light. We further discuss additional predictive results from, and details of, these simulations including low-order aberrations in § 8.3 & § 8.4. In § 9 we make specific recommendations in light of the VCT #5 experimental results, informing the model simulations, for (in the future) ultimate full attainment of milestone 2.

8.3 Low Order Aberrations

The EXCEDE starlight suppression system has a LOWFS to measure low-order aberrations with commands sent to the DM for their correction. In this technology demonstration, the low-order aberrations that are sensed and corrected are the tip/tilt modes. In post-facto model simulations, we introduce defocus and astigmatism aberration modes in proportions that match the shape of the experimental PSF as defined by maximizing a cross-correlation function; then the total magnitude of low-order aberrations is determined by a comparison to the measured on-axis system Strehl ratio.

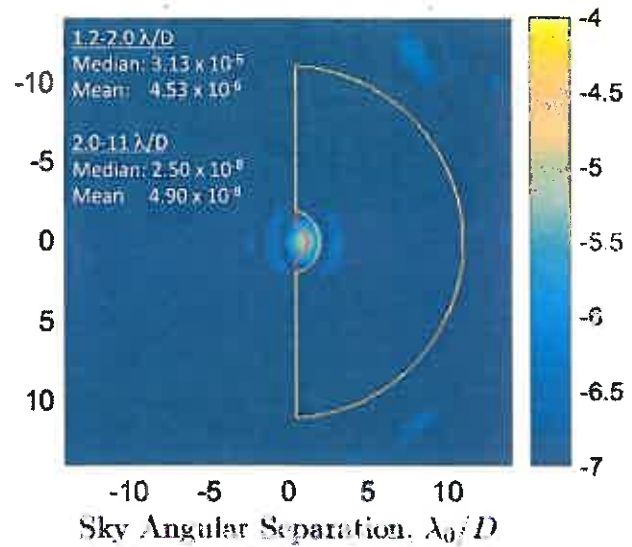


Fig. 14: Ideal performance of EXCEDE starlight suppression system with SN WF correction.

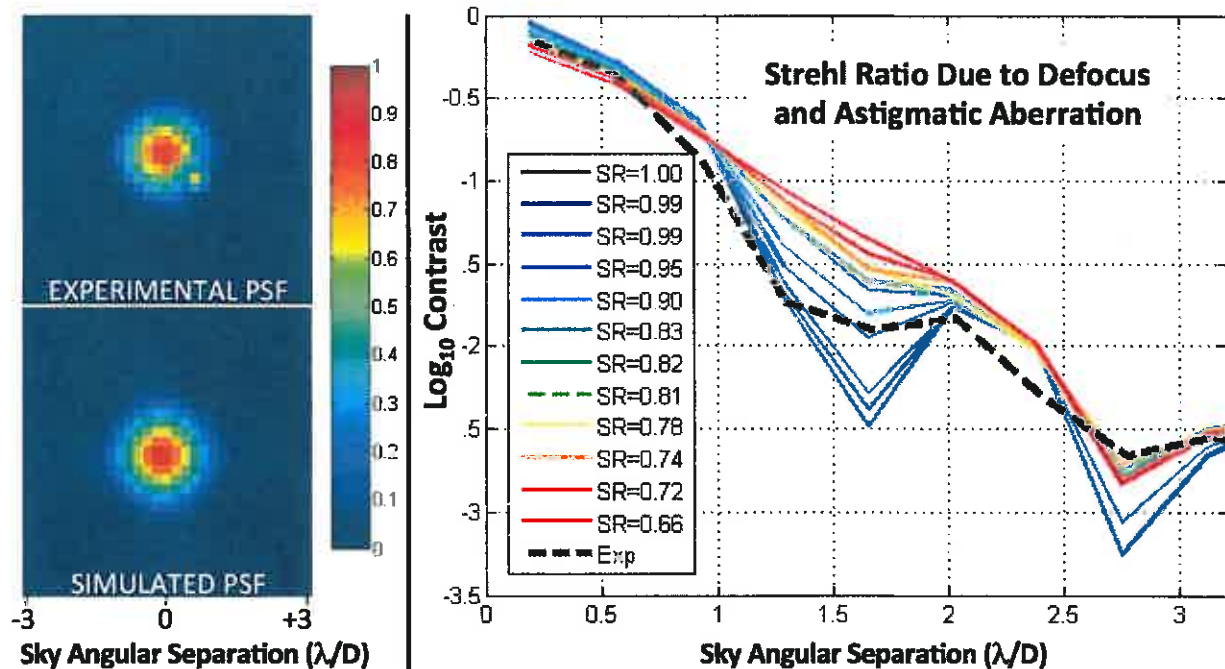


Fig. 15: Left: Experimentally measured and best-correlation simulated on-axis PSF ($SR = 0.81$). Right: 360° radial profiles comparing different simulated PSFs with the experimental PSF (dashed line).

In Figure 15 (left), we compare images of the experimental PSF with a simulated PSF having combined astigmatism and defocus terms for which a best correlation match is found with a Strehl ratio of 0.81. We also show (right) 360° azimuthally averaged radial profiles of the experimental and simulated PSFs showing the effect on Strehl ratio and to contrast with induced defocus and astigmatism.

The resulting phase aberration map applied at the PIAA M1 plane is shown in Figure 16. These aberrations correspond to RMS amplitude 0.8 radians, with the dominating aberration being the oblique astigmatism added.

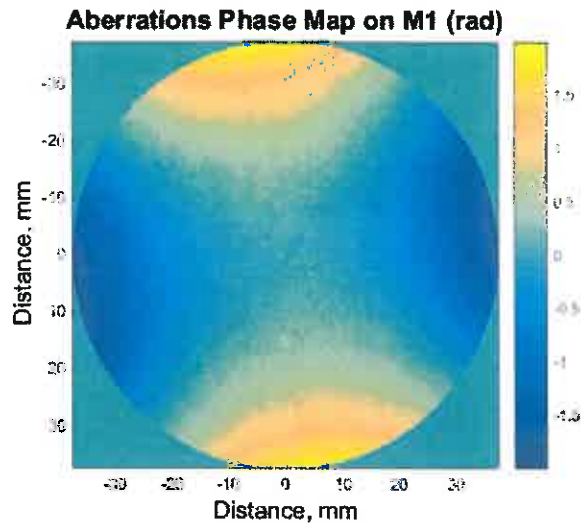


Fig. 16: Corresponding phase aberrations introduced on the PIAA M1.

The cause of these astigmatic aberrations remains somewhat speculative. We suggest that the most likely source is due to misalignment between the front-end OAPs. For our MS #2 testing, the optical alignment of the testbed was performed in air, then tested in vacuum, and misalignment (particularly between the OAPs) plausibly was introduced by the change of environment from air to vacuum.

8.4. Simulation results.

To determine the effect of the low-order aberrations on the performance of the EXCEDE starlight suppression system, we perform a simulation similar to the ideal case that established a performance baseline. In particular, we apply the low-order aberrations matched to the measured experimental PSF as described in the previous section together with $\lambda/20$ surface aberrations as expected from the optical surfaces.

The result of this simulation is shown in Figure 17 (left). We compare this result with one of the representative experimental milestone results in Figure 17 (right). The contrast in the IWZ is limited by the diffracted light at the center of the image. The shape and intensity of this diffracted light is related to the low-order aberrations present in the system. Whereas our model is relatively simple and assumes all the aberrations are collocated at M1, we can observe important qualitative similarities between the simulation and experiment. Specifically, the bright spot in the center has two dimmer companion spots in both cases; this is due to the oblique astigmatism term whereas a pure horizontal astigmatism aberration results in only two such spots. The location of the spot is matched to that of the experiment by the inner working angle verification routine – when the mask is set such that the IWA is located at $1.2 \lambda/D$, the centroid of the simulated diffraction spot is the same as that observed in the experiment. The ringing structure around this bright spot is at a similar scale (approximately Airy 4 rings out to $5 \lambda/D$), and this is given by matching the size of the Lyot stop between experiment and simulation. The contrast field structure in the OWZ is better controlled beyond $5 \lambda/D$ in simulation that may be explained by convergence differences between the simulated wavefront

control algorithm that uses perfect knowledge of the electric field and the experimental implementation.

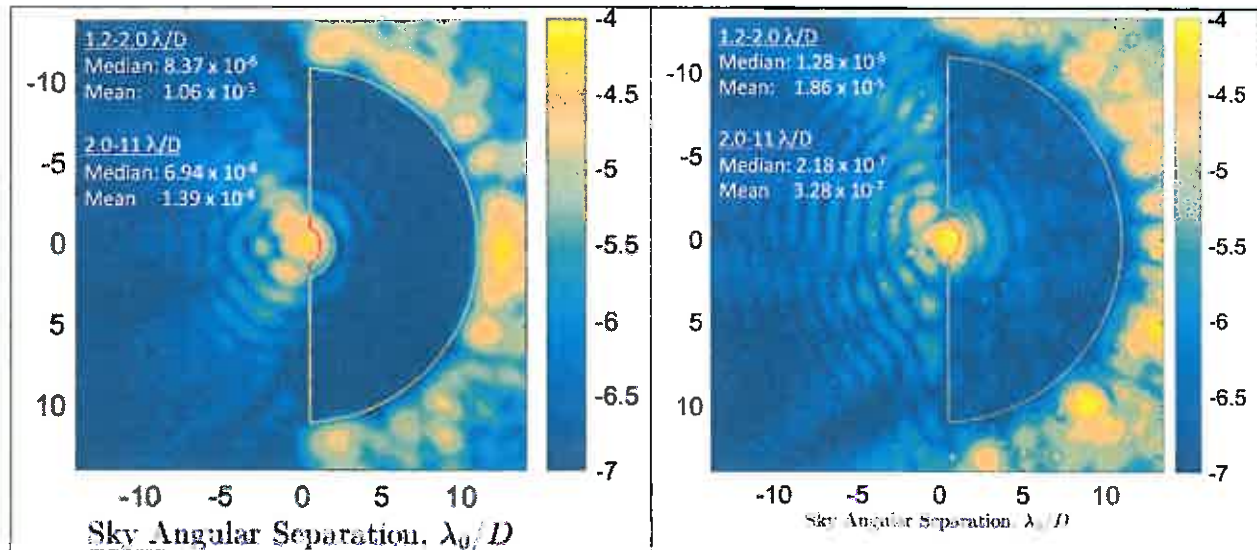


Fig. 17: Performance comparison of the EXCEDE SSS in simulation (left) with experiment (right).

8.4.1. Sensitivity to Tip/Tilt

We also perform a sensitivity analysis with respect to a residual tip/tilt term. No tip/tilt terms were added with the low-order aberrations, but after performing wavefront control and obtaining an optimal DM setting we add residual tip/tilt¹⁶ to determine the robustness of the solution to small tip/tilt deviations. Because of the number of iterations involved in a typical experimental run and the integration times, it is likely that some residual misalignment may develop.

The results of the sensitivity to residual tilt are shown in Figure 18. The monochromatic simulation at the corrected wavelength shows more sensitivity to residual tilt because it is starting from a deeper contrast that degrades more quickly. The broadband curve shows that the IWZ median contrast is limited at $\sim 10^{-5}$ obtained in the experiment for residual tilt on the order of $0.015 \lambda/D$. This amount of tilt may appear large because it is on the same order as the amount of tilt being removed by the tip/tilt correction from the LOWFS. However, the actual residual tip/tilt is dynamic and a typical milestone run occurred over the course of an entire day – a smaller but dynamic residual tip/tilt could provide similar performance degradation. Drifts in the absolute position of the focal plane mask on the order of $0.015 \lambda/D$ are within the uncertainty of the mask verification procedure¹⁷.

We can estimate the approximate effect of the residual tilt in a second way through the monochromatic curve. The monochromatic curve is of interest because in the test bed the IWZ cannot be corrected to better than 10^{-5} without engaging the LOWFS. Additionally, the final

¹⁶ Implemented as "single-shot" tilts; i.e., in the "horizontal" direction.

¹⁷ What's important are dynamic variations relative to the LOWFS setpoint, even if that setpoint happens to be 0.015 off the optical axis.

corrected monochromatic performance is on the order of 3×10^{-6} . This corresponds to roughly the same $0.015 \lambda/D$ residual tilt for which the broadband IWZ contrast is at $\sim 10^{-5}$.

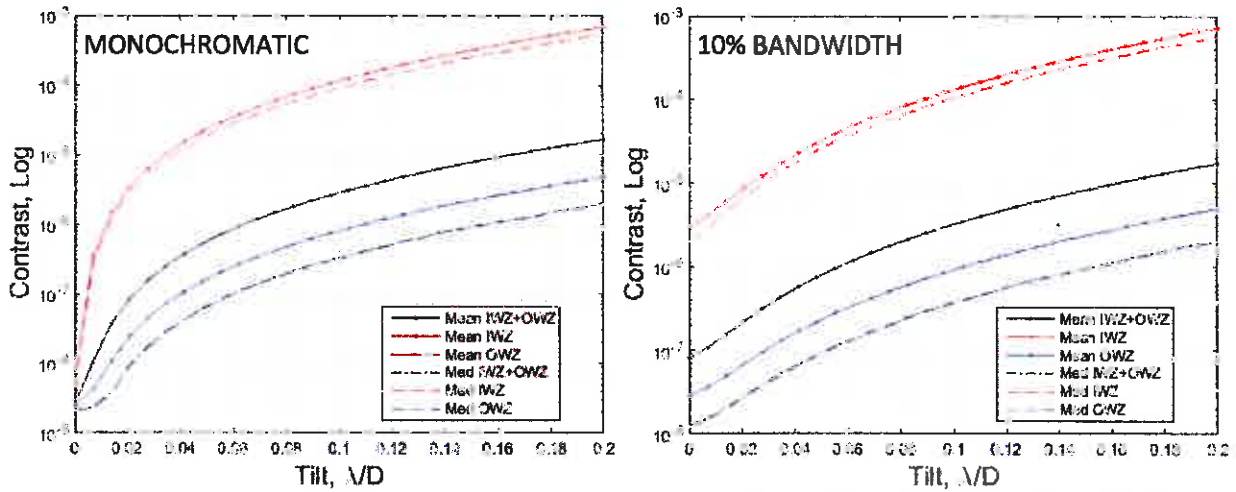


Fig. 18: Contrast performance with residual tilt for monochromatic and 10% broadband light.

8.4.2. Contrast Degradation with Increasing Bandwidth

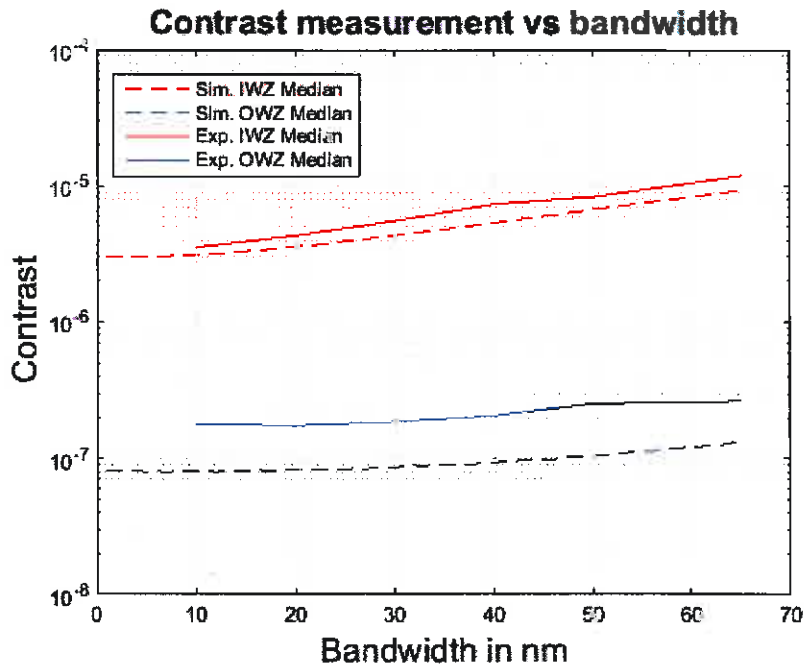


Fig. 19: Comparison of median contrast as a function of input light bandwidth between model and experiment for both IWZ and OWZ.

Although not part of the MS #2 10% bandwidth contrast demonstration, we explored the degradation in contrast with increasing bandwidth. We posed the question as to whether the observed degradation can be explained by the model? We computed the IWZ and OWZ median contrast by maintaining the obtained monochromatic DM settings gradually increasing the filter bandwidth from 10 nm (1.5%; the minimum tunable setting beyond monochromatic in

our test configuration) up to 65 nm (corresponding to 10% light) or vice-versa. This was also done in simulation. The comparison is shown in Figure 19. For the IWZ, we have a factor of 3 degradation of contrast from 10 nm to 65 nm in the test bed that is matched by simulation. The degradation in contrast for increased bandwidths is more pronounced for the IWZ than for the OWZ.

8.4.3. Simulated Comparison of Wavefront Control Algorithms: SN vs. EFC

Although the MS #2 demonstration runs were conducted using SN exclusively (see § 6.1), in simulation we performed and compared the results of both SN (where a perfect model of the system was assumed) and EFC (where perfect knowledge of the electric field was assumed); e.g. see Figure 20. Both the qualitative and quantitative matches we obtained between the two algorithms, and to the performance of laboratory experiment, reinforces our conclusion that we are limited by physical factors and not limited by (different) implicit assumptions in either WF control algorithm.

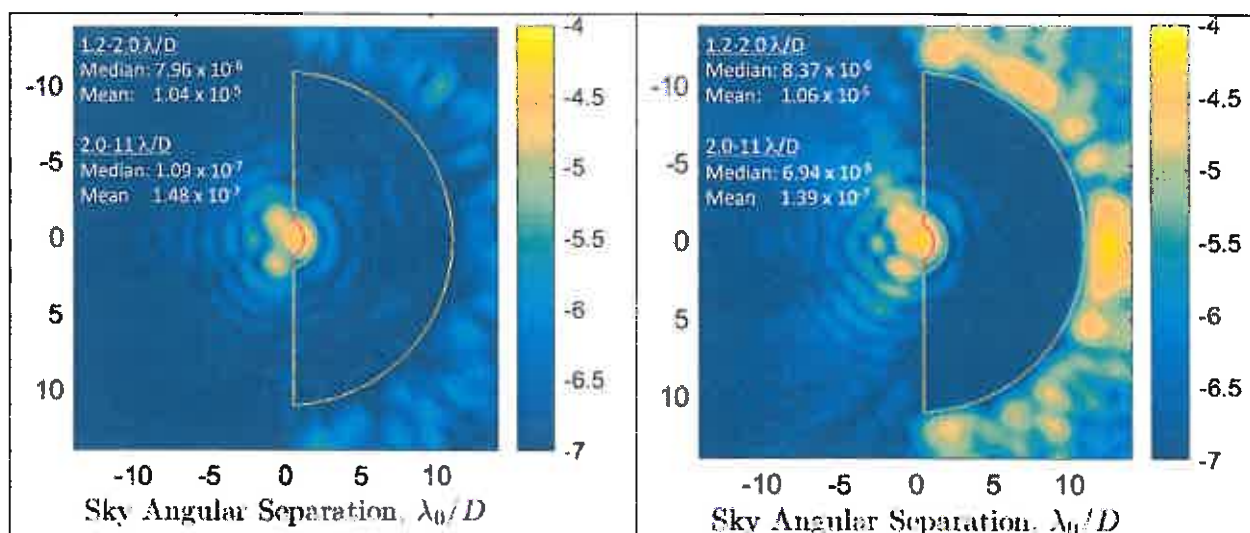


Fig. 20: Comparison in simulation of SN (left) to EFC (right) in 10% broadband light both realistically modeling the experimental system with low-order aberrations per § 8.3 included.

9. What Next? -- Meeting the Milestone

There are multiple ways in which the EXCEDE SSS could be improved for broadband light performance, in particular for deeper image contrast in the IWZ. First, the first generation forward PIAA optics (Axsys mirror system) that we used for this technology demonstration were non-optimal. In particular they were: (1) designed for $2 \lambda/D$ IWA and, (2) not designed for broadband light. In future developments, we recommend using a PIAA system specifically designed to match the proposed EXCEDE stellocentric angles and broadband wavelengths.

Second, we investigated, through post-facto modeling, ways in which performance for the *current* system (as tested with the 1st generation Axsys mirrors) can be improved – without investing in new laboratory PIAA optics.

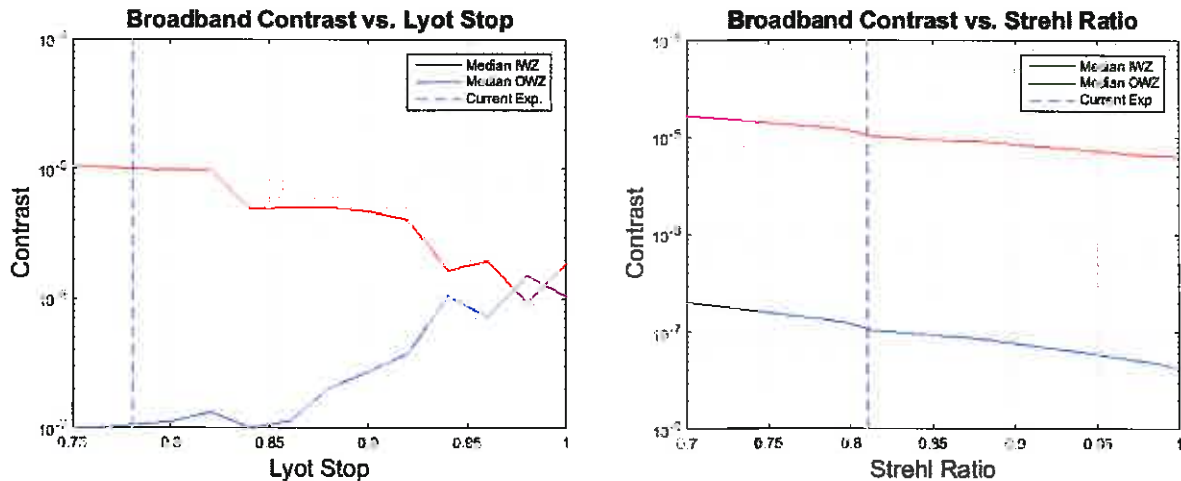


Fig. 21: Predicted contrast performance: Left (a) - as a function of Lyot stop opening diameter (s ; $s = 1.00$ is fully open) while keeping the magnitude of the aberrations on M1 fixed. Right (b) - as a function of Strehl ratio while maintaining the current Lyot stop opening ($s = 0.78$). (The dashed lines indicate the Lyot stop opening and Strehl ratio for the current experimental setup.)

Using the model of our test bed, we have found that the IWZ milestone contrast can be met under the following combined conditions:

- Opening the Lyot stop beyond the experimentally considered range (clear diameter $s > 0.85$, where $s = 1.00$ is fully open).
- Maintaining a Strehl ratio ≥ 0.9 (vs. experimentally maintained at 0.81-0.85)
- Maintaining a residual tilt $\leq 0.015 \lambda/D$.

Below, we speak to each:

(a) As shown in Figure 21 (left panel), a performance improvement in the IWZ may be obtained by opening the Lyot stop. The light blocked by the Lyot stop primarily corresponds to higher spatial frequency light and thus to light in the Outer Working Zone. On the other hand, opening the Lyot stop increases the size of the exit pupil, thus reducing the broadening of the central diffraction features that limit contrast in the Inner Working Zone. In this experiment, we are currently contrast limited in the IWZ. We predict that by opening the Lyot stop beyond $s = 0.85$ (currently $s = 0.78$) IWZ contrast would improve as shown in Fig 21 (with order of magnitude improvement fully

open). However, beyond $s = 0.85$ the OWZ contrast is predicted to degrade. In combination, along with an expectation of predicted contrast improvement in both zones with increasing Strehl ratio (see (b) below and, e.g., Figure 21 right panel), future experimentation (given still remaining uncertainties in the model) can explore the trades in this Lyot stop size/Strehl ratio parameter space to optimize the performance in both zones, and inform a (yet) higher fidelity model.

(b) As shown in Figure 21 (right panel), a performance improvement in both zones may be obtained by maintaining Strehl ratios higher than experimentally tested. To achieve this we propose/anticipate (in future testing) a change in the procedure (rather than in hardware). To date, the experimental Strehl ratio has been ascertained in air prior to pumping down to vacuum. We propose, in the future, that the Strehl ratio be measured in vacuum prior to starting each wavefront control run. To achieve this more aggressive Strehl ratio (e.g., > 0.9), further testing on all the optical mounts and surfaces in vacuum may be required to ensure that misalignments are not induced by the vacuum environment. Additionally, with an upstream DM (as configured for the MS #2 demonstration), appropriate actuators can (also) be used to compensate for the dominating low-order astigmatism term (currently this is not done); the LOWFS can be used to measure these additional Zernike modes to be corrected.

(c) The $0.015 \lambda/D$ residual tilt is derived from the sensitivity analysis as a current limiting factor. We maintain this same residual tilt, but further reductions of this residual tilt would result in improved contrast performance.

In Figure 22 we predictively illustrate the combined effect (improvement in contrast performance) with (a) Lyot stop fully open ($s = 1.0$), (b) Strehl ratio = 0.9, and (c) residual tilt = $0.15 \lambda/D$, using our realistic (aberrated) model of the system, and current (existing) PIAA optics.

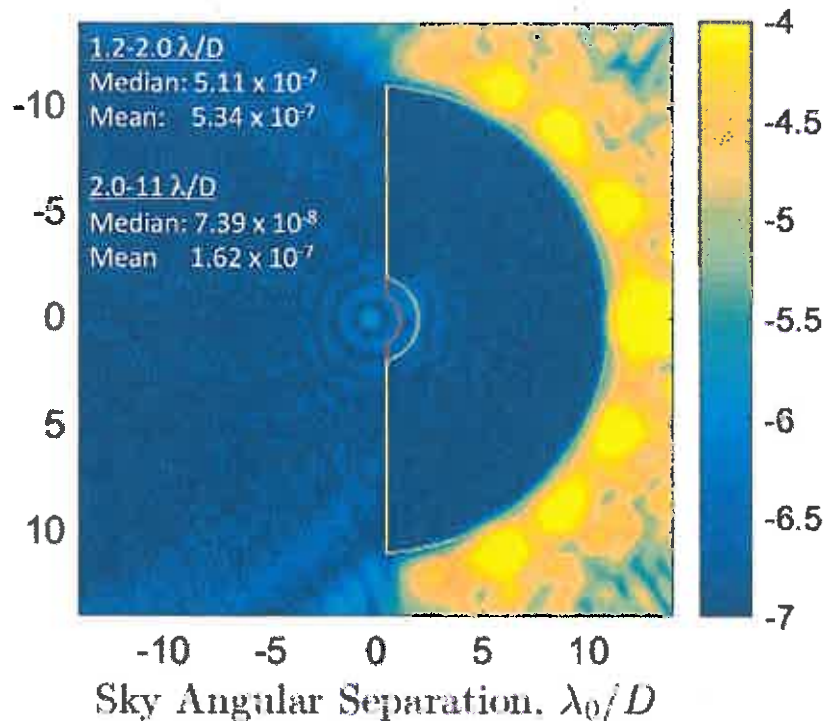


Fig. 22: Simulation of performance for the proposed improved criteria. Both the IWZ and OWZ are predicted to better than meet the milestone #2 contrast goals simultaneously.

10. Summary and Conclusion

• **(A):** The EXCEDE test bed starlight suppression system, integrating those key elements identified in Table 5 of the flight mission proposal for TRL maturation:

- PIAA optics for high contrast coronagraphy,
- Deformable Mirror for mid-spatial frequency wavefront control,
- Low-order wavefront sensing,
- Wavefront control algorithms,

has been operationally demonstrated in a vacuum environment ($\approx 3 \times 10^{-6}$ Torr) relevant to the EXCEDE mission's proposed low-Earth orbit (closely approaching TRL 5 with the exception of (C), as discussed below).

(A) meets the charge to the EXCEDE Project by NASA/HQ and Explorer Program Office category III funded investigation, as articulated in §1 of this report.

• **(B):** The EXCEDE MS #2 raw median contrast goal for 10% spectral bandwidth was attained and robustly demonstrated in the OWZ from 2.0 – 11.0 λ/D (98% of the dark zone controlled area).

(B) enables the EXCEDE flight concept science requirements (to $\leq 11 \lambda/D$ tested) per the EXCEDE STM IFRs reproduced in Appendix A (entries in green).

However,

• **(C):** The EXCEDE MS #2 raw median contrast goal for 10% spectral bandwidth with simultaneous imaging in the IWZ from 1.2 – 2.0 λ/D (innermost 2% of the dark zone controlled area, ≤ 0.8 resels beyond the FPM edge) was not obtained by approximately an order of magnitude. The reasons for this are believed understood, and validated models (§ 8) show how to achieve this milestone (§ 9), as demonstrable in a future vacuum test.

Context of (B) and (C) for the proposed EXCEDE science and mission concept:

(B): The $\leq 3 \times 10^{-7}$, 10% broadband, contrast goal obtained in the $> 2 \lambda/D$ OWZ is better than the EXCEDE Instrument Functional Requirement (IFR), as documented in the flight proposal Science Traceability Matrix (replicated in Appendix A), by a factor of 3 or more for all relevant science goals. We continue, however, to strive for deeper contrasts still in the OWZ commensurate with changes in the system configuration suggested as necessary to attain (C), as validated models suggest (e.g., Fig. 21).

(C): There is no IFR for EXCEDE contrast performance inward of 2 λ/D . However, to enable value-added science beyond the mission threshold criteria we established a more technically challenging additional goal for our TM&D milestones with also 10^{-6} raw median contrast in a 1.2 – 2.0 λ/D interior zone. This goal was met for monochromatic light (milestone #1) but, as discussed in § 7 & 9, not (yet) achieved with the EXCEDE test bench as configured for the VCT #5 milestone #2 demonstration.

• **(D):** Through modeling and simulation compared to vacuum laboratory experimentation, specific achievable pathways have been identified to future attainment of (C); see § 9. This is the logical next step for the further maturation of capabilities enabled with the EXCEDE starlight suppression system.

11. References

- [Bel12a] Belikov, R., Pluzhnik, E., Witteborn, F., Greene, Thomas P., Lynch, Dana H., Zell, Peter T., Schneider, G., Guyon, O., Tenerelli, D. 2012, "EXCEDE technology development I: first demonstrations of high contrast at $1.2 \lambda/D$ for an Explorer space telescope mission", Proceedings of the SPIE, Volume 8442, article id. 844209;
<http://adsabs.harvard.edu/abs/2012SPIE.8442E..09B>
- [Bel12b] Belikov, R., Pluzhnik, E., Lozi, J., Witteborn, F., Greene, T., Lynch, D., Schneider, G., Guyon, O., Tenerelli, D. 2013, "EXCEDE Technology Development: Demonstrations of High Contrast at $1.2 \lambda/D$ and Fast Low-order Wavefront Control for an Explorer Space Telescope Mission", American Astronomical Society, AAS Meeting #221, #305.02;
<http://adsabs.harvard.edu/abs/2013AAS...22130502B>
- [Bel13b] Belikov, R., Bendek E., Greene, T., Guyon, O., Lozi, J., Lynch, D., Newman, K., Pluzhnik, E., Schneider, G., Tenerelli, D., Thomas, S., Witteborn, F. 2013, "EXCEDE Technology Development II: demonstration of high contrast at $1.2 \lambda/D$ and preliminary broadband results", Proceedings of the SPIE, Volume 8864, article id. 88640;
<http://spie.org/Publications/Proceedings/Paper/10.1117/12.2024569>
- [Bel13a] Belikov, R., Lozi, J., Pluzhnik, E., Hix, T., Bendek, E., Thomas, S., Lynch, D., Mihara, R., Irwin, J., Duncan, A., Greene, T., Guyon, O., Kendrick, R., Smith, E., Witteborn, F., Schneider, G. 2013, "EXCEDE technology development III: first vacuum tests", Proceedings of the SPIE, Volume 9143, id. 914323;
<http://proceedings.spiedigitallibrary.org/proceeding.aspx?articleid=1894793>
- [Ben14] Bendek, E., Belikov, R., Lozi, J., Schneider, G., Thomas, S., Pluzhnik, E., Lynch, D. 2014, "Optomechanical design of the vacuum compatible EXCEDE's mission testbed", Proceedings of the SPIE, Volume 9143, id. 91435D;
<http://proceedings.spiedigitallibrary.org/proceeding.aspx?articleid=1894894>
- [Guy05] Guyon, O., Pluzhnik, E., Galicher, R., Martinache, F., Ridgway, S., Woodruff, R. 2005, "Exoplanet Imaging with a Phase-induced Amplitude Apodization Coronagraph. I. Principle" ApJ, 622, 744-758;
<http://iopscience.iop.org/0004-637X/622/1/744/pdf/61515.web.pdf>
- [Guy12] Guyon, O., Schneider, G., Belikov, R., Tenerelli, D. 2012, "The EXoplanetary Circumstellar Disk Environments and Disk Explorer", Proceedings of the SPIE, Volume 8442, id. 1362241;
<http://proceedings.spiedigitallibrary.org/proceeding.aspx?articleid=1362241>
- [Loz13] Lozi, J., Belikov, R., Schneider, G., Guyon, O., Pluzhnik, E., Thomas, S., Martinache, F. 2013, "Experimental study of the low-order wavefront sensor for the high-contrast coronagraphic imager EXCEDE", Proceedings of the SPIE, 8864, id. 886400;
<http://proceedings.spiedigitallibrary.org/proceeding.aspx?articleid=1744168>
- [Loz14] Lozi, J., Belikov, R., Thomas, S., Pluzhnik, E., Bendek, E., Guyon, O., Schneider, G., 2014, "Experimental Study of a Low-Order Wavefront Sensor for High-Contrast Coronagraphic Imagers: Results in Air and Vacuum", Proceedings of the SPIE, Volume 9143, article id. 914322;

<http://proceedings.spiedigitallibrary.org/proceeding.aspx?articleid=1894792>

- [Nor09] Norton, Thomas, S., 2009,
https://exep.jpl.nasa.gov/files/exep/EXCEDE_Milestone_1_01DEC2012_GS09.pdf
- [Sch12] Schneider, G., Guyon, O., Belikov, R., Greene, T., Tenerelli, D. 2012, “EXCEDE Technology Milestone #1: Monochromatic Contrast Demonstration”, JPL Document D-75787;
https://exep.jpl.nasa.gov/files/exep/EXCEDE_Milestone_1_01DEC2012_GS09.pdf
- [Sch12a] Schneider, G., EXCEDE team, 2012, “The EXoplanetary Circumstellar Disk Environments and Disk Explorer”, American Astronomical Society, AAS Meeting #219, #155.13;
http://nicmosis.as.arizona.edu:8000/POSTERS/AAS_JAN2012_EXCEDE_AS_PRINTED.pdf
- [Sch13] Schneider, G., Belikov, R., Thomas, S., Pluzhnik, E., Davis, P., Lynch, D., Greene, T., Guyon, O., Smith, E. 2013, “EXCEDE Technology Milestone #1: Monochromatic Contrast Demonstration Completion Report”, JPL Document D-81372;
http://exep.jpl.nasa.gov/files/exep/EXCEDE_MILESTONE1_CLOSURE_REPORT_02DEC2013_V06.pdf
- [Sch15] Schneider, G., Lozi, J., Guyon, O., Newman, K., Belikov, Lynch, D., Zell, Thomas, S., Pluzhnik, E., Witteborn, F., Bendek, E., Hix, T., Nordt, A., 2015, “EXCEDE Technology Milestone #2: Broadband Contrast Demonstration”, JPL Document D-94365;
http://exep.jpl.nasa.gov/technology/POST-TAC_EXCEDE_Milestone_2_R_020_NOTFLAGGED.pdf

APPENDIX A – EXCEDE Flight Proposal Science Traceability Matrix (STM)

Science Goals & Objectvs.	Scientific Measurement Requirements		Instrument Functional Requirements		Projected Performance	Top-Level Mission Functional Req's
	Observables	Physical parameters				
Goal I,III Sci Obj. 1 What are dust levels in HZ's of exoplanetary Systems?	Surface brightness	Surf. density	Raw Contrast	10^{-6} resel ⁻¹ @ 2-28 λ /D, either λ	10^{-7} resel ⁻¹ @ 1.2-30 λ /D	3 yr mission for ~350 target survey
	Substructure Morphology Extent	Spatial Scale	IWA OWAC ^a OWAU ^a	2 λ /D, either λ 15 λ /D, either λ 80 λ /D, either λ	1.2 λ /D 30 λ /D 150 λ /D	
			Spatial. Res.	288 mas	144 mas	
Disk Color	Composition	Spec. Bands	0.4, 0.8 μ m \pm 20% R=10-20%	0.4, 0.8 μ m; R=20%		
Goal I,II Sci. Obj. 2 Interference with planet-finding?	Surface brightness	Surf. density	Raw Contrast	10^{-6} resel ⁻¹ @ 2-28 λ /D, either λ	10^{-7} resel ⁻¹ @ 1.2-30 λ /D	sun synchronous dawn/dusk orbit for anti-sun target viewing and thermal stability
	Substructure Morphology	Spatial Scale	IWA OWAC	2 λ /D, either λ 15 λ /D, either λ	1.2 λ /D 30 λ /D	
			Spatial. Res.	288 mas	144 mas	
Goals I,III Sci. Obj. 3 What veneer is delivered to planets by asteroids and comets?	Surface brightness	Surf. density	Raw Contrast	10^{-6} resel ⁻¹ @ 2-28 λ /D, either λ	10^{-7} resel ⁻¹ @ 1.2-30 λ /D	maintain stellar image on LOWFS focal plane mask
	Location	Stellocentric Distance	IWA OWAC OWAU	2 λ /D, either λ 15 λ /D, either λ 80 λ /D, either λ	1.2 λ /D 30 λ /D 150 λ /D	
			Spatial. Res.	288 mas	144 mas	
	Polarization	Stokes u,q,p, θ	Accuracy, σ P%	5%, 2% resel ⁻¹	1%, 1% resel ⁻¹	
Grain Color	Composition	Spec Bands	0.4, 0.8 μ m \pm 20% R=10-20%	0.4, 0.8 μ m; R=20%		
Goal II,III Sci. Obj. 4 Large orbit massive planet prevalence?	Surface brightness	Surf. density	Raw Contrast	10^{-6} resel ⁻¹ @ 2-28 λ /D, either λ	10^{-7} resel ⁻¹ @ 1.2-30 λ /D	2000 km orbit for large CVZ target scheduling efficiency
	Substructure Morphology Extent	Location and Spatial Scale	IWA OWAC OWAU	2 λ /D, either λ 15 λ /D, either λ 80 λ /D, either λ	1.2 λ /D 30 λ /D 150 λ /D	
			Spatial. Res.	288 mas	144 mas	
Goal II,III Sci. Obj. 5 How do PP disks make Solar System like architectures?	Surface brightness ^c	Surf. density	Raw Contrast	10^{-6} resel ⁻¹ @ 2 λ /D, either λ	10^{-7} resel ⁻¹ @ 1.2-30 λ /D	ONR capability for non-CVZ and multiple-orientation observations
	Substructure Morphology Extent	Spatial Scale	IWA OWAC OWAU	2 λ /D, either λ 15 λ /D, either λ 80 λ /D, either λ	1.2 λ /D 30 λ /D 150 λ /D	
			Spatial. Res.	288 mas	144 mas	
	Polarization	Stokes u,q,p, θ	Accuracy, σ P%	5%, 2% resel ⁻¹	1%, 1% resel ⁻¹	
Disk Color	Composition	Spec. Bands	0.4, 0.8 μ m \pm 20% R=10-20%	0.4, 0.8 μ m; R=20%		
Goal II, III Sci Obj. 6 Albedos & compositions of cool giant exoplanets?	Brightness & Albedo	Flux Density	Raw Contrast	10^{-6} resel ⁻¹ @ 2-15 λ /D, either λ	10^{-7} resel ⁻¹ @ 1.2-30 λ /D	
	Polarization	Stokes u,q,p, θ	Accuracy, σ P%	5%, 2% resel ⁻¹	1%, 1% resel ⁻¹	
	Location	Orbit. Dist. and P.A.	IWA OWAC ^c OWAU ^c	2 λ /D, either λ 15 λ /D, either λ 80 λ /D, either λ	1.2 λ /D 30 λ /D 150 λ /D	
Spatial. Res.			288 mas	144 mas		

^a OWAC = High contrast outer WA controlled by DM; OWAU = uncontrolled: full imaging field size beyond OWAC.

IFRs relevant to this milestone investigation are highlighted in the above table.

APPENDIX B – SOURCE CALIBRATION USING THE LOWFS

In order to calibrate an image in dimensionless units of image contrast, the raw images need to be normalized by the peak intensity of the unocculted PSF¹⁸. However, due to the limited dynamic range of the detectors, the setting used to image the unocculted PSF and the ones for the coronagraphic image differ significantly in both exposure time and source configuration. For the laser used in the ACE laboratory for our MS #1 demonstration, the calibration of the source was automated as the Labview software remotely controlled the source. However, the broadband source of the supercontinuum laser used for the MS #2 demonstration can only be controlled manually and the source calibration, in this case, is not automatic. The protocol for the supercontinuum source calibration, however, is straightforward using the LOWFS.

The LOWFS has an option to look at the flux ratio between the reference PSF and the live PSF (e.g., Figure 22, bottom right display), or the flux ratio when changing the source brightness and the exposure time. The tool used for this purpose is at the bottom graph showing the flux. If the "normalized" button at the top is checked, the flux varies slightly around unity. If not, then the flux value gives the ratio between the actual source flux and as measured in the reference.

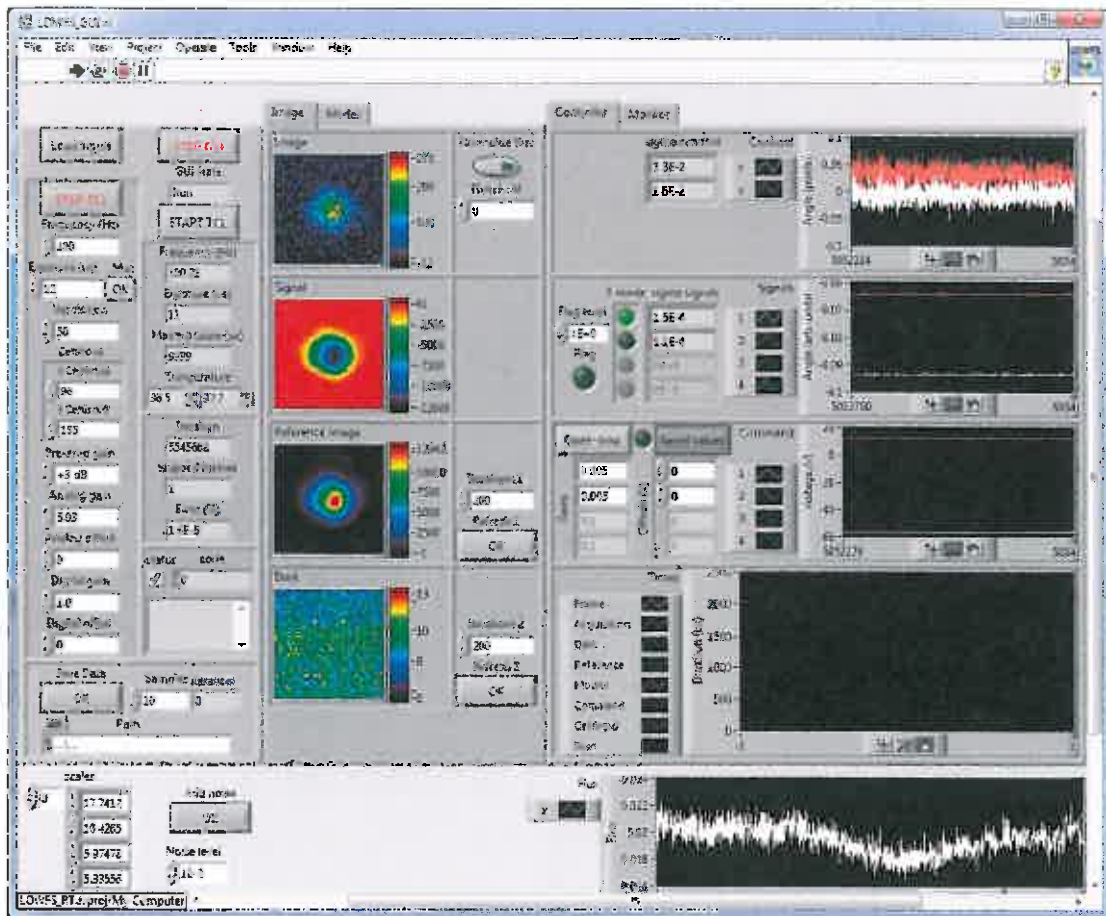


Fig. 22: LOWFS graphical user interface.

¹⁸ Throughout this investigation, we have defined the image contrast as the of the flux density contained within a pixel (or resel) at any stellocentric location in the PSF halo of a coronagraphically occulted source ratioed to the peak flux density within the central pixel (or resel) of the unocculted PSF core.

Therefore, to calibrate the source as a function of bandwidth or power we follow the following steps:

- Set the reference PSF using the setting for the unocculted PSF (5% power, 10nm bandwidth around 650nm). The measured flux is the reference.
- Change the power of the source to 50% and then 100%.
- For each power, adjust the exposure time using the LOWFS GUI and measure the intensity ratio. Adjust the measured ratio for the difference in exposure time. This gives the normalization factor to go from the raw coronagraphic image to the contrast image as a function of source power.
- To get the normalization factor as a function of bandwidth, one needs to do the same when changing the bandwidth to 20nm, 30nm, 40nm, 50nm and 65nm.

The following table shows the normalization factor for the different configurations. As mentioned above, the reference image has a power source of 5% and a bandwidth of 10nm. The average taken for the final results is shown on the right.

Power Level (%)	Bandwidth (nm)	Normalization for different measurements			Average	Standard deviation
5	10	1	1		1	
50	10	0.101683168	0.107181136		0.104432152	0.00388765
100	10	0.05213198	0.055	0.051970823	0.053034267	0.00170428
100	20	0.024697395		0.025559406	0.025128401	0.000609534
100	30	0.016716175		0.016947007	0.016831591	0.000163223
100	40	0.012511675		0.012573586	0.012542631	4.37777E-05
100	50	0.010068627		0.009994389	0.010031508	5.24945E-05
100	65	0.007847182		0.007795623	0.007821403	3.64577E-05
5	65	0.163015873			0.163015873	

For all the milestone runs, the unocculted PSF was measured with 5% power level and a bandwidth of 10nm to make sure the image was not saturated with the shortest exposure time. The final coronagraphic images are measured with a 100% power level and a 65nm bandwidth. Therefore, the normalization factor is $7.8214 \times 10^{-3} \pm 5.25 \times 10^{-5}$. This factor is used in the Matlab code `batch_milestone_###.m` (included in the data certification package).

APPENDIX C– Electronic Certification Data Package and Summary

Per § 6.1 of JPL D-94365, we provide in electronic form the raw and calibrated imaging and ancillary data and calibration files used to derive the contrast field maps and stability plots representatively illustrated in Figure 11. This electronically downloadable Certification Data Package has been prepared and is available to the NASA Exoplanet Exploration Office for independent review and/or analysis¹⁹. This is in compliance with § 4.2 of the aforementioned guiding document.

In addition to materials presented in this report, the electronic Certification Data Package includes:

- (I) the Matlab codes used to create the graphs presented in the written report.
- (II) the MEMS characterization data.
- (III) the contrast field and DM voltage data for all certification test runs.

(I) Matlab codes - under CODES directory.

This section presents a list of source codes that were used during the calibration process and the data reduction process. There are 2 sets of codes:

- The MEMSCodes:
 - o DM_flat.m: measures the map of the MEMS that will provide a flat wavefront
 - o DM_deflection.m: measures the deflection curve
 - o InfluenceFunction.m: measure the influence function of 3 specific actuators.
 - o Depiston.m, detilt.m and my_centroid.m are helpers codes
 - o Read_zygo_xyz.m: code to read the zygo images files.
- The MilestoneRunCodes:
 - o Batch_milestone_runA.m: allows to create the average final contrast as well as the stability graphs for run A
 - o Batch_milestone_runB.m: allows to create the average final contrast as well as the stability graphs for run B
 - o Batch_milestone_runC.m: allows to create the average final contrast as well as the stability graphs for run C

(II) Data

All the data corresponding to a particular VCT #5 test id (A, B, or C) stored in a folder with the letter designation (TestA, TestB, or TestC).

(A) MEMS Calibration Data

These data are located in the folder (under Data) called DMTestingdata. There are 2 subfolders DeflectionCurveData and FlatData:

- DeflectionCurveData: This folder gathered the data used to measure the deflection curve.

¹⁹ Access information to a UofA server hosting the CDP for electronic download via sftp is separately provided to the NASA EXEP office.

- Deflection.bmp: This is the map of the known pattern used to calculate the deflection curve.
- L_xyz: zip files containing the data at different voltage level to calculate the deflection curve. Numbers in the file names are correspond to encoded voltages in Zygo format read through the procedure Read_zygo_xyz,m in the Codes/MEMSCodes directory (1 volt = 224.2 ADU in file name; linear)
- FlatData: This folder collects the Calibration data (Calib subfolder) and the measurement data (V140 subfolder).
 - Geometry_calibration.bmp: map of the known pattern sent to the mirror in order to measure the plate scale and the orientation of the DM relative to the Zygo instrument.
 - HEX_Volt.dat: conversion between hexadecimal values and voltages to be sent to the mirror
 - Def.mat and Definv.mat: deflection results coming from the previous folder.
 - Geom.xyz: measurement from the zygo instrument. Uses read_zygo.m to read the files.
 - FinalFlat.fits: This file is the map of the voltages to apply to the MEMS to correct for its own aberrations. (The Strehl ratio after applying this correction was >90%; alone not in the end-to-end system).

(B) Instrumental Calibration Data

The instrumental calibration data generated through the procedures discussed in § 5 of this report are archived in the CDP for each test run. The ## in the file names correspond to the test run numbers as shown in Fig 12. We archive in the CDP these calibration files in the corresponding Images subdirectory as follows:

1- Image_Run00##_Fiber_alignment.fits: This is a cube of 40 images, 20 images corresponding to a displacement of the fiber in x and 20 images corresponding to a displacement of the fiber in y.

2- Image_Run00XX_InvPIAA_alignment.fits: This aligns the inverse PIAA using the LOWFS camera.

3- Image_Run00##_Calibration.fits: This is a cube of 50 images, representing five different configurations for which we took 10 images. The first 10 images are just the PSF (to measure the peak intensity of the core PSF). The next 40 images are four different sets of sine waves put on the DM to measure the plate scale of the camera relative to the MEMS and the centering of the PSF. Each of the four sets contains 10 images.

4- Image_Run00##_IWA_Calibration.fits: This is a cube of 40 images, 20 images corresponding to a displacement of the mask in x and 20 images corresponding to a displacement of the mask in y.

5- Image_Run00##_IWA_Verification.fits: This is a cube of 20 images corresponding to a displacement of the fiber in x only.

6 & 7-: At the beginning of each run dark frames were taken for both the LOWFS camera archived in CDP images called *Dark_Run00##_Imperx.fits*, and for the science camera called: *Dark_Run00##_QSI.fits*.

(C) Contrast Field and DM Voltages

Image_Run00##_IterXXXX.fits: The contrast field images for each test run (##), with ≥ 1000 measured sequential iterations of the contrast field acquired with SN wavefront control.

DMVoltages_Run00##_IterXXXX.fits: Voltages applied to the DM actuators (32x32 map) during SN at each iteration corresponding to the contrast field image.

(III) CDP Directory Structure

The directory structure for all the data files contained within the electronic CDP (under the top level directory called MS2_CDP) is shown below.



APPENDIX D – Comments on the Coronagraph Optical Model

IMPROVEMENT (over pre-test model): Three major improvements were made to the coronagraph optical model from pre-test to post-test:

- (1) Addition of an inverse PIAA numerical propagator. This propagator was verified against the expected theoretical PSF (and a numerical artifact was identified and corrected).
- (2) Inclusion of a simulated mask alignment procedure identical to the bench procedure (§ 5.5) that ensures the IWA is at $1.2 \lambda/D$ in the model. Previously, the default mask location corresponded to the 50% throughput at $1.0 \lambda/D$, which resulted in a more optimistic prediction especially for the broadband performance.
- (3) Matching of the modeled PSF to a more realistic experimental PSF. We still do not fully understand the physical cause of the experimental aberrations (see §8.3), but after having performed the experiment we have a more realistic estimate of the impact on performance than from *a priori* modeling.

VALIDATION: To our knowledge, ours is the first PIAA experiment pushing into the $1.2 \lambda/D$ IWA regime, and so this was the first opportunity to test/validate the end-to-end model described in § 8 experimentally. While this end-to-end model has (also) not been tested against other simulation codes, its components have been (e.g., PIAA propagators, models of masks, and Fraunhofer propagation between non-PIAA optics). Previous PIAA configurations, using these pieces, have been validated by experiment, and geometrical propagation vs. diffraction has been validated in simulations. In particular, the geometrical remapping method has been validated against other PIAA propagators (geometrical remapping with Talbot effect correction which simulates diffraction, Fresnel diffraction, S-Huygens diffraction) with the following conclusions: (1) For on-axis modes with no errors, geometrical remapping gives the same result (down to 10^{-10} contrast level) as long as the edges of the pupil are feathered with a pre (or post-) apodizer. (2) Without apodizers, the results are correct to $\sim 10^{-7}$ contrast level. (3) For low-order modes (tip/tilt, defocus, etc.) the results are similar. (4) For higher order modes, the shape of the speckle field in the focal plane starts deviating between geometrical remapping and other models, *but the contrast levels remain the same*.

→ Therefore, for principal purpose of determining the contrast of the speckles (as opposed to exact morphology), geometrical remapping should be a sufficient model.

N.B.: Although we do not know all of the factors limiting $1.2 - 2.0 \lambda/D$ (IWZ) contrast to 10^{-5} in the lab, the model correspondingly shows contrast limited to 10^{-5} – at least for the effects that the model considered.

APPENDIX E – ACRONYM LIST

ACE	Ames Coronagraph Experiment
ARC	Ames Research Center
BMC	Boston Micromachines Corporation
CDP	Calibration Data Package
DM	Deformable Mirror
EFC	Electric Field Conjugation
EXCEDE	EXoplanetary Circumstellar Environments & Disk Explorer
EXEP	EXoplanet Exploration Program
FITS	Flexible Image Transport System
FPM	Focal Plane Mask
GUI	Graphical User Interface
IFR	Instrument Functional Requirement
IWA	Inner Working Angle (in λ/D , arcseconds, or milliarcseconds)
IWZ	Inner Working Zone
JPL	Jet Propulsion Laboratory
L3 / L4	(inverse PIAA) Lens 3 or Lens 4
LM	Lockheed-Martin
LOWFS	Low Order Wave Front Sensor
M1 / M2	Mirror 1 or 2: referring to PIAA mirrors used in pairs
MEMS	Micro Electro-Mechanical Systems
MET	Metrology Environment Test
MS	Milestone
NASA	National Aeronautics and Space Administration
OAP	Off-Axis Paraboloid
OWA	Outer Working Angle (in λ/D , arcseconds, or milliarcseconds)
OWZ	Outer Working Zone
PI	Principal Investigator
PIAA	Phase Induced Amplitude Apodized
PSF	Point Spread Function
SN	Speckle Nulling
SSS	Starlight Suppression System
S/W	Software
TMA	Three Mirror Anastigmat
TM&D	Technology Maturation and Demonstration
TRL	Technology Readiness Level
VCT	Vacuum Chamber Test
WF	Wavefront
WFC	Wavefront Control
WFE	Wavefront Error
WP	Whitepaper